ORGANOMETALLICS

pubs.acs.org/Organometallics

Article

Ylide-Substituted Phosphines with a Cyclic Ylide-Backbone: Angle Dependence of the Donor Strength

Julian Löffler, Richard M. Gauld, Kai-Stephan Feichtner, Ilja Rodstein, Jana-Alina Zur, Jens Handelmann, Christopher Schwarz, and Viktoria H. Gessner*

Cite This: *Organometallics* 2021, 40, 2888–2900

Read Online

ACCESS | Metrics & More | Article Recommendations | Supporting Information

ABSTRACT: Ylide-substituted phosphines (YPhos) have been shown to be highly electron-rich and efficient ligands in a variety of palladium catalyzed transformations. Here, the synthesis and characterization of novel YPhos ligands containing a cyclic backbone architecture are reported. The ligands are easily synthesized from a cyclic phosphonium salt and the chlorophosphines Cy_2PCl (**L1**) and $Cy(Flu^{Me})PCl$ (**L2**, with Flu^{Me} = 9-methylfluorenyl) and were characterized in both solution and solid states. The smaller PCy_2-substituted ligand, **L1**, readily formed the biscoordinate $\mathbf{L1_2Pd}$ species when treated with $Pd_2(dba)_3$ and showed no activity in palladium-catalyzed amination reactions even when applied as defined palladium(II) η^3-allyl, *t*-Bu-indenyl, or cinnamyl precursors. Bulkier fluorenyl-substituted ligand **L2** similarly was inactive, despite its ability to form the stable monophosphine complex **L2**·Pd(dba). Assessment of the electronic properties by experimental and computational methods revealed that **L1** and **L2** are considerably less electron-rich than previously synthesized YPhos ligands. This was shown to be the result of the small P−C−S bond angle, which is sterically enforced due to the cyclic nature of the backbone. Density functional theory calculations revealed that the small angle results in an increased s-character of the lone pair at the ylidic carbon atom and leads to a polarization of the C−P bond toward the carbon atom, thus decreasing the electron density at the phosphorus atom. The results demonstrate the tunability of the donor strength of YPhos ligands by modification of the ligand backbone beyond simple changes of the substitution pattern and are thus important for future ligand design, with a careful balance of many factors to be considered to achieve catalytic activity.

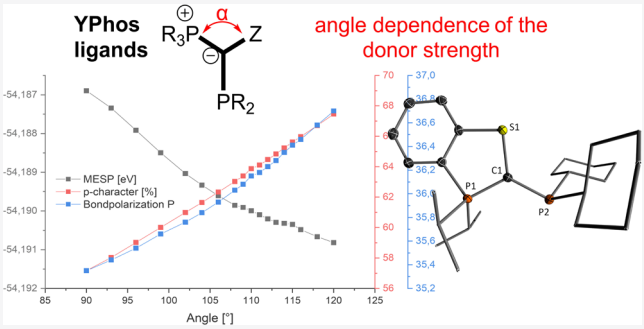

INTRODUCTION

Phosphines are a privileged class of ligands ubiquitous in homogeneous catalysis, a vital cornerstone of modern synthetic chemistry, with applications ranging from large-scale pharmaceuticals to fine stereo control of complex natural products.[1−3] Although extensive research efforts have focused on *N*-heterocyclic carbenes (NHCs) as ligand systems in the past few decades due to their in general higher electron-donating properties when compared with phosphines, phosphines remain the ligand systems of choice for many applications. This continuing popularity is due to several reasons, including the simplicity of their synthesis, generally from commercially available starting materials, and the wide breadth of possible substitution patterns, which allows for the precise control of the phosphines electronic and steric properties, enabling the fine-tuning of the phosphine properties toward a desired purpose. Several advances in homogeneous catalysis over previous decades have been driven by this fact.[4,5] For systematic ligand design various metrics are used in order to describe the electronic and steric properties of phosphine ligands, including the Tolman electronic parameter (TEP),[6,7] cone angle, and the buried volume.[8] These measures facilitate the understanding of structure activity relationships in catalysis and build the foundation to computer-aided catalyst design.[9]

In the past years, many research efforts have focused on the preparation of highly electron-rich phosphines due to their beneficial properties for late transition metal catalysis. For a long time, trialkyl phosphines particularly with tertiary alkyl substituents such as *t*-Bu or Ad (Ad = adamantyl) groups were the phosphines ligands with the highest donor strength. For example, Carrow and co-workers synthesized tri(1-adamantyl)-phosphine, PAd_3, and impressively demonstrated its applicability in palladium catalysis.[10] However, other substituents at phosphorus also have been applied in past years to further increase the donor strength. Thus, Dielmann and co-workers

Received: June 11, 2021
Published: August 4, 2021

reported on the use of imidazolidin-2-imino substituents (IAPs),[11] and Sundermeyer and co-workers on phosphazenyl groups (PAPs) to access super basic phosphines (Figure 1).[12] Their donor capacity can compete with or even surpass that of NHCs, demonstrating the electronic flexibility of specially designed phosphine ligands.

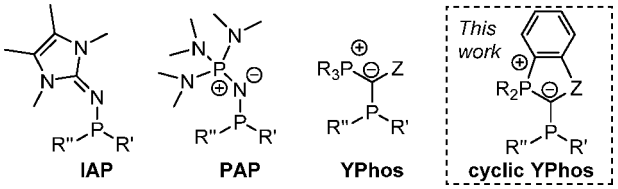

Figure 1. Examples of highly electron-rich phosphines.

Recently, our group reported on ylide-substituted phosphines (YPhos), which feature an ylide group directly bonded to the phosphorus center.[13] As a result of this ylide group and its strong electron-donating abilities, these phosphines exhibited strong electron-donating capabilities, with donor capacities surpassing those of simple phosphines and NHCs. These ligands were shown to be ideal scaffolds for catalytic applications, ranging from gold-catalyzed hydroamination and cyclization reactions[14] to palladium catalysis, such as Buchwald–Hartwig aminations as well as Negishi couplings and α-arylation reactions under mild conditions.[15] Recently, it has been shown that YPhos palladium catalysts are even capable of directly coupling aryl chlorides and alkyl lithium reagents, giving very high selectivities while supplementing the need for any additional transmetalation reagents.[16]

Due to the efficiency of YPhos ligands in catalysis, we became interested in a more profound understanding of the impact of the ligand architecture on the catalytic ability. In this contribution, we showcase the development of a new class of YPhos ligands with a cyclic ylide functionality and demonstrate that this cyclic structure has a decisive impact on the electronic properties.

RESULTS AND DISCUSSION

Ligand and Complex Syntheses and Catalytic Studies. In order to synthesize a cyclic YPhos ligand, we selected easily accessible phosphonium salt **1** as the first test system. We initially set out to synthesize corresponding dicyclohexylphosphine **L1** in order to allow for comparison with previously synthesized YPhos ligands. Phosphonium salt [**1**]I could be obtained in 57% yield in a one-pot reaction of 2 equiv of *n*BuLi and TMEDA with thiophenol, followed by the slow addition of di-*iso*-propylchlorophosphine to give an *ortho*-phosphino thiolate, which was subsequently cyclized via diiodomethane addition (Figure 2). The successful formation of [**1**]I could be confirmed by a singlet at δ_p = 76.5 ppm in the $^{31}P\{^1H\}$ NMR spectrum and by XRD analysis (see the Supporting Information for further details). The structure shows a distorted five-membered ring, with a slight deviation of the phosphorus center out of the plane (Figure 2). Starting from [**1**]I, the corresponding ylide could be isolated in near-quantitative yields by treatment with strong, sterically demanding metal bases such as KHMDS or KO*t*-Bu. Deprotonation using such bases in THF afforded ylide **2** within 1 h. Attempted deprotonation using other bases such as *n*BuLi or KH resulted in the formation of a mixture of

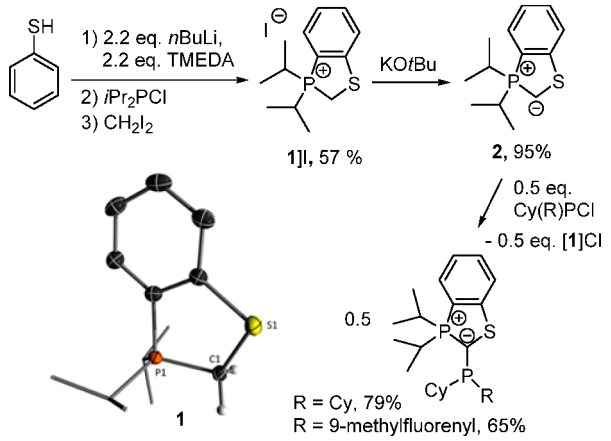

Figure 2. Synthesis of the YPhos ligands **L1** and **L2** with a cyclic ylide backbone and molecular structures of the cation of **1**. Ellipsoids drawn at 50% probability level; hydrogen atoms omitted for clarity. Selected bond lengths [Å] and angles [°]: P(1)–C(1) 1.803(2), S(1)–C(1) 1.824(2), P(1)–C(1)–S(1) 108.3(1).

products, likely due to unwanted deprotonation of the CH group of the isopropyl moiety. The ylide is a dark red oil at room temperature, characterized by a high-field-shifted signal at δ_p = 50.2 ppm in the $^{31}P\{^1H\}$ NMR spectrum. In keeping with the reactivity of ylide species, exposure of the solution to air resulted in the formation of a decomposition product, in which the phosphonium moiety is oxidized to phosphine oxide, with the concomitant loss of the bridging carbon atom between the sulfur and phosphorus centers (see the Supporting Information). Attempts to obtain the corresponding yldiide of **2** by using a second equivalent of a strong metal base were unsuccessful, even with the use of strong bases such as $NaNH_2$, KHMDS, or benzyl potassium and at elevated temperatures.

With the ylide in hand, desired ligand **L1** was synthesized by slow addition of 0.5 equiv of Cy_2PCl to **2**. Thereby, the ylide acts as reagent and base, thus leading to the re-formation of the chloride salt of **1** ([**1**]Cl) and final ligand **L1**. Within the synthesis pathway, formation of an α-phosphino-substituted phosphonium salt was never observed, suggesting that its deprotonation to **L1** by ylide **2** is a fast process. After removal of [**1**]Cl by filtration ([**1**]Cl being reobtained in 82% yield), **L1** was obtained as orange solid in 79% yield. Analysis via $^{31}P\{^1H\}$ NMR spectroscopy showed a set of doublets at δ_p = 50.7 ppm for the phosphonium group and at δ_p = −14.9 ppm for the phosphine moiety with a coupling constant of $^2J_{pp}$ = 108.6 Hz. Recrystallization from hot acetonitrile furnished crystals suitable for XRD analysis, which confirmed the connectivity of the new ligand (Figure 3).

Next, the ability of phosphine **L1** in palladium catalysis was tested by means of Buchwald–Hartwig aminations. The reactions were carried out using 4-bromotoluene and 4-chlorotoluene as electrophiles and *n*-butylamine and *N*-methylaniline as amines with 3 mol % of Pd_2dba_3 and free ligand, both at room temperature and 50 °C.[17] After a period of 24 h, the reaction mixture was analyzed by GC analysis, revealing no detectable conversion for any substrate combination. This contrasts the high activity of the acyclic YPhos ligands which provided high yields in these reactions at room temperature usually within only a couple of minutes.[15,16]

To understand the origin of the inactivity of **L1**, we set out to examine its steric and electronic properties. Reaction of the new ligand with (tht)AuCl allowed us to obtain the

https://doi.org/10.1021/acs.organomet.1c00349
Organometallics 2021, 40, 2888–2900

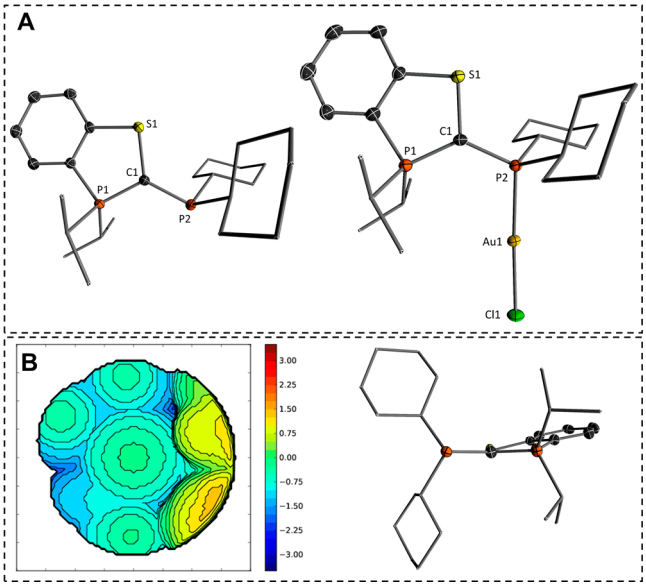

Figure 3. (A) Molecular structures of **L1** and **L1·AuCl**; ellipsoids are drawn at a 50% probability level. Hydrogen atoms are omitted for clarity. Selected bond lengths [Å] and angles [°]: **L1**: P1−C1 1.7077(12), S1−C1 1.7920(12), C1−P2 1.7746(12), P1−C1−S1 111.44(6), P1−C1−P2 124.43(7). **L1·AuCl**: P1−C1 1.717(2), S1−C1 1.793(1), C1−P2 1.754(2), P2−Au1 2.248(1), Au1−Cl1 2.303(1), P1−C1−S1 112.7(1), P1−C1−P2 130.0(1). (B) Steric map of **L1** derived from **L1·AuCl** using the SambVca 2.0 (P−M distance of 2.28 Å including H atoms).[18]

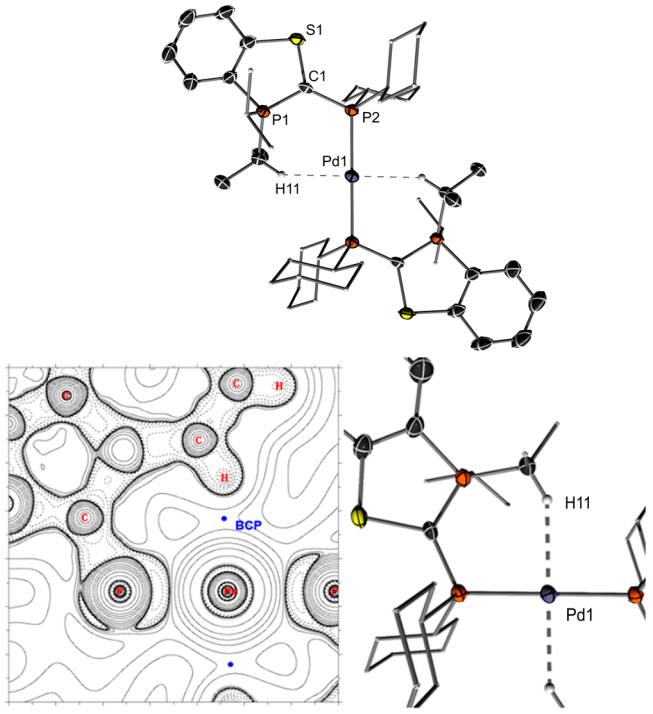

Figure 4. (Top) Molecular structure of $\mathbf{L1_2Pd}$; ellipsoids are drawn at a 50% probability level. Hydrogen atoms are omitted for clarity. Selected bond lengths [Å] and angles [°]: P(1)−C(1) 1.706(3), S(1)−C(1) 1.796(3), C(1)−P(2) 1.766(3), P(1)−Pd(1) 2.300(1), Pd(1)−H(11) 2.44(3), P(1)−C(1)−S(1) 110.9(1), P(1)−C(1)−P(2) 126.4(1), P(2)−Pd(1)−H(11) 88.59(2). (Bottom left) Contour-line diagram of the Laplacian distribution of $\mathbf{L1_2Pd}$. Solid lines indicate charge depletions [$\nabla^2\rho(r) > 0$]; dashed lines indicate charge concentrations [$\nabla^2\rho(r) < 0$]. (Bottom right) Section of the molecular structure of $\mathbf{L1_2Pd}$.

corresponding gold complex in 73% yield, which was fully characterized by various analytical methods, including XRD analysis (see the Experimental Section for full details). The obtained molecular structure of **L1·AuCl** shows a slight shortening of the C1−P2 bond [1.754(2) Å] upon coordination of the metal [1.775(1) Å in **L1**], as expected. The P1−C1−P2 angle increases from 124.43(7) to 130.0(1)°, thus reducing steric repulsion between the *i*Pr groups and the gold center (Figure 3). From this structure, the buried volume was calculated using SambVca.[18] The obtained buried volume of 42.5% is lower than that of other acyclic YPhos ligands with PCy_3 or PPh_3 moieties, which usually showed volumes of approximately 50%.[13−15] Furthermore, the steric map of **L1** shows areas of steric bulk only on one side of the of the ligand, namely, the phosphonium moiety. The cyclohexyl groups are unable to reach toward the metal center. This observation suggests, that **L1** might be too small to efficiently stabilize the monoligated LPd species and instead leads to the formation of the corresponding bisphosphine complex L_2Pd, which have been shown to be inactive in catalysis.[16,19]

To prove this hypothesis, we attempted the isolation of palladium complexes with **L1**. Reaction of **L1** with $Pd_2(dba)_3$ resulted in instantaneous formation of a new species, detected via $^{31}P\{^1H\}$ NMR spectroscopy. The NMR spectrum showed a set of two doublets at δ_p = 53.6 and 13.1 ppm. The reaction reached full conversion within 10 min, and the resulting bisphosphine ligated complex could be isolated in high yields of 81%. Crystallization from pentane and THF confirmed the formation of the L_2Pd species (Figure 4). While the formation of such complexes was found to be hampered with the acyclic YPhos ligands reported earlier,[16] **L1** readily forms the bisphosphine species because of its low steric bulk. In the molecular structure, the palladium lies on the inversion center between the two phosphine atoms, with the P(2)−Pd(1) bond of 2.300(1) Å being shorter than the one found for the acyclic keYPhos ligand, $Cy_3PC(Me)PCy_2$, featuring a PCy_3 moiety (2.332(6) Å).[16] Also of interest is the observation of a short Pd(1)−H(11) distance of only 2.47(3) Å between the palladium and the hydrogen atom of an *i*Pr group. Thus, the palladium center adopts a pseudo-square-planar geometry. The bonding nature of the Pd−H interaction was also confirmed by DFT calculations. QT/AIM studies showed the presence of a bond critical point between the Pd and H atoms, suggesting the presence of a stabilizing interaction. Such interactions have been previously observed with the keYPhos ligand; however, in the latter case a slightly larger distance of 2.52(3) Å was observed.[15a,16]

As previously shown via mechanistic studies, monoligated PdL species are the active catalysts in a plethora of palladium-catalyzed reactions involving bulky monophosphines, while in contrast the PdL_2 species are often considered as catalytically inactive.[16,19] To prevent the formation of PdL_2 defined precatalysts featuring a ligand to metal ratio of 1:1 have been designed to facilitate the formation of catalytically active Pd species and inhibit the formation of PdL_2.[20] Prominent examples of such monophosphine systems include η^3-allyl, *t*-Bu-indenyl, and cinnamyl complexes.[21] In this vein, precatalysts of **L1** based on the η^3-allyl, cinnamyl, and *t*-Bu-indenyl complexes were synthesized (Scheme 1) by mixing of the free ligand and the dimeric palladium precursors in pentane giving the three desired complexes ($\mathbf{Pd_{al}1}$, $\mathbf{Pd_{cin}1}$, and $\mathbf{Pd_{ind}1}$)

https://doi.org/10.1021/acs.organomet.1c00349
Organometallics 2021, 40, 2888−2900

Scheme 1. Synthesis of the Palladium Complexes with L1 and L2

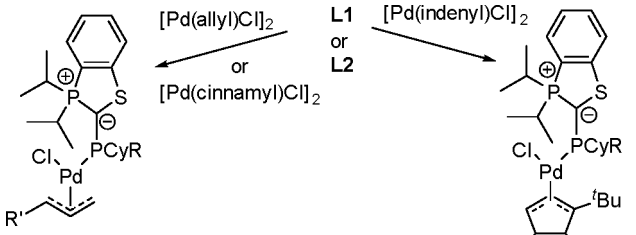

$Pd_{al}1$, R = Cy, R´ = H, 73 %
$Pd_{al}2$, R = Flu^{Me}, R´ = H, 72 %

$Pd_{cin}1$, R = Cy, R' = Ph, 76 %
$Pd_{cin}2$, R = Flu^{Me}, R' = Ph, 55 %

$Pd_{ind}1$, R = Cy, 66 %
$Pd_{ind}2$, R = Flu^{Me}, 84 %

in good yields directly from solution. In all three cases, NMR spectroscopic analysis shows one set of doublets with similar shifts in the $^{31}P\{^{1}H\}$ NMR spectrum, with the resonances for the phosphonium moiety appearing at approximately δ_p = 56 ppm and for the phosphine moiety between δ_p = 20.3 and 27.0 ppm. Structural analysis was carried out on $Pd_{cin}1$ and $Pd_{ind}1$, with both showing shortened carbon−phosphorus bonds [1.7563(3) and 1.720(2) Å] and larger P(1)−C(1)−P(2) angles [130.0(2) and 130.1(1)°] compared to the free ligand. The isolated palladium complexes were not only applied in BHA but also showed no activity under the reaction conditions mentioned above.

We also attempted to crystallize the Pd−allyl complex; however, we were instead only able to obtain a decomposition product (Figure 5), in which a second phosphonium moiety is formed through substitution of the allyl group from the Pd−allyl precursor together with $[Pd(allyl)Cl_2]^-$ as counterion. Formation of this species is very slow, with only small quantities formed after several days in solution, thus excluding that this decomposition reaction is the reason for the catalytic activity of **L1**.

We then assessed the electronic properties of the dicyclohexyl ligand by measurement of the CO stretching vibration in [**L1**·Rh(acac)(CO)]. Correlation with stretching frequencies in $LNi(CO)_3$ complexes yielded a TEP of 2057.1 cm^{-1}. This value is surprisingly high compared with other YPhos ligands, which usually featured high donor strengths similar to carbenes. For example, the acyclic YPhos ligands keYPhos with a PCy_3 moiety and a methyl group in the ylide backbone exhibited a TEP value of 2050.1 cm^{-1}.[12] The high TEP value of **L1** was further confirmed by DFT calculations. To this end, the minimum of the molecular electrostatic potential (MESP) at the phosphorus atom was calculated and correlated with the TEP, a method previously described by Suresh and Koga.[22] This method yielded a TEP_{ESP} of 2057.1 cm^{-1}, thus corroborating with the experimentally obtained value.

To understand whether the catalytic inactivity of the palladium complexes of **L1** is due to the low steric demand or the weak donor strength, we accessed an analogues ligand to **L1** with a bulkier phosphine moiety containing a 9-methylfluorenyl substituent. The fluorenyl group was expected to further expand toward the coordination sphere of the metal and thus impede the formation of the detrimental L_2Pd species. New ligand **L2** was synthesized from in situ formed ylide **2** and ClPCyFlu, which was made from 9-methylfluorene ($Flu^{Me}H$, see the Supporting Information)[23] by deprotonation with *n*BuLi and slow addition to a solution of cyclohexyldichlorophosphine at −60 °C. Similar to **L1**, slow addition of 0.5 equiv of the chlorophosphine to **2** directly gave way to final ligand **L2**, which was obtained as a yellow solid in 65% yield after purification. **L2** is characterized by a set of doublets at δ_p = 52.0 and 12.2 ppm with a coupling constant of $^{2}J_{PP}$ = 119.5 Hz in the $^{31}P\{^{1}H\}$ NMR spectrum. Recrystallizing from hot acetonitrile furnished single crystals of **L2** suitable for single-crystal XRD analysis (Figure 6). The ligand adopts the desired conformation, whereby the fluorenyl substituent is directed toward the coordination site of the phosphine. Thus, **L2** appears to be bulkier than **L1**. The P1−C20 bond length, which is that between the fluorenyl and the phosphine, amounts to 1.927(1) Å and is thus relatively long when compared to typical bonds between phosphorus and an alkyl group (e.g., P2−C14 1.847(1) Å). In contrast, the P1−

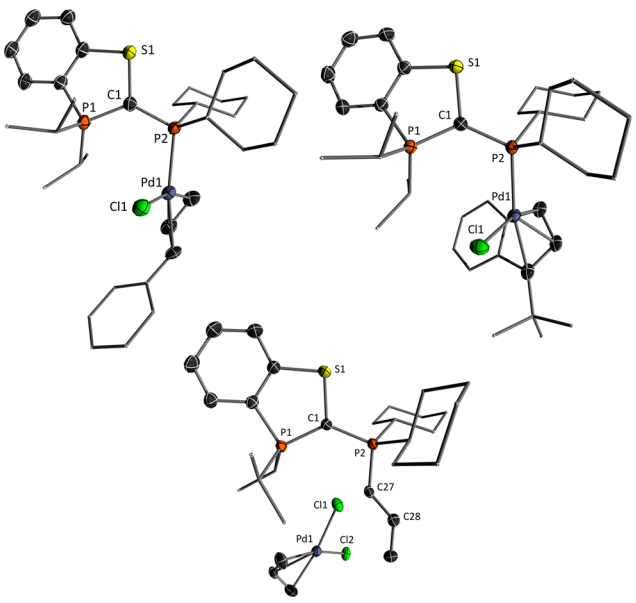

Figure 5. (Top) Molecular structures of (left) $Pd_{cin}1$ and (right) $Pd_{ind}2$ with ellipsoids drawn at a 50% probability level. Hydrogen atoms are omitted for clarity. Selected bond lengths [Å] and angles [°]: $Pd_{cin}1$: P1−C1 1.715(3), S1−C1 1.791(3), C1−P2 1.756(3), P2−Pd1 2.306(1), Pd1−Cl1 2.365(1), P1−C1−S1 111.1(1), P1−C1−P2 130.0(2). $Pd_{ind}1$: P1−C1 1.720(2), S1−C1 1.796(2), C1−P2 1.756(2), P2−Pd1 2.283(1), Pd1−Cl1 2.376(1), P1−C1−S1 110.4(1), P1−C1−P2 130.1(1). (Bottom) Molecular structure of decomposition product of $Pd_{al}1$.

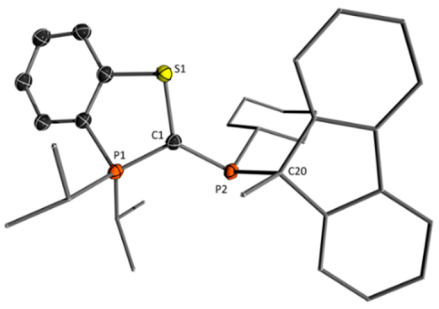

Figure 6. Molecular structure of **L2**. Selected bond lengths [Å] and angles [°]: P1−C1 1.713(1), S1−C1 1.794(1), C1−P2 1.761(1), P2−C20 1.927(1), P1−C1−S1 109.5(1), P1−C1−P2 124.5(1).

https://doi.org/10.1021/acs.organomet.1c00349
Organometallics 2021, 40, 2888−2900

C1−P2 bond angle of 124.5(1)° is similar to that in **L1** and thus seems to be unaffected by the increased bulk of the fluorenyl group.

To gain further insights into the steric properties of **L2** we attempted the synthesis of the gold chloride complex in order to determine the buried volume, $\%V_{bur}$. Reaction with (tht)AuCl resulted in the formation of a new species, as detected by NMR spectroscopic studies. We were able to observe a set of doublets in the $^{31}P\{^{1}H\}$ NMR spectrum at δ_p = 58.4 and 44.7 ppm, with a coupling constant of $^{2}J_{pp}$ = 57.4 Hz. However, due to rapid decomposition in solution, isolation of this species was not possible. Thus, we right away focused on the synthesis of palladium complexes with **L2**. The reaction of **L2** with $Pd_2(dba)_3$ gave way to two species. The first of these was identified as bisphosphine complex **L2$_2$Pd**, which showed the characteristic coupling pattern with a set of two doublets at δ_p = 52.0 and 38.8 ppm in the $^{31}P\{^{1}H\}$ NMR spectrum, similar to **L1$_2$Pd**. Unambiguous identification came from XRD analysis (Figure 7). Unfortunately, disorder within

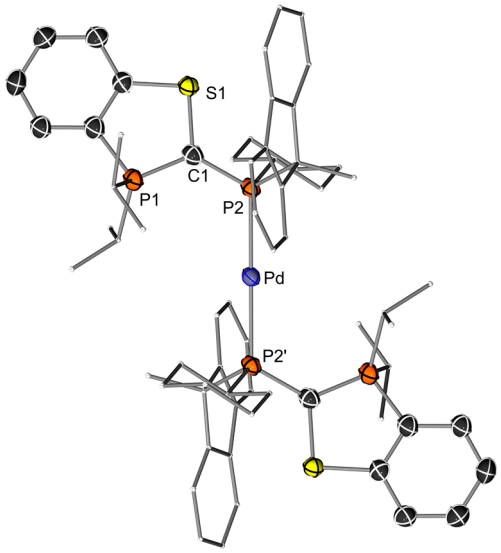

Figure 7. Molecular structure of **L2$_2$Pd** with ellipsoids drawn at 50% probability level. Hydrogen atoms are omitted for clarity.

the structure prevented a detailed discussion of bond lengths and angles, but the molecular connectivity is unambiguous. Of note is the change in conformation of the fluorenyl group when compared to the free ligand. Presumably, this change is instrumental to allow two ligands to coordinate to the Pd(0) center.

As a consequence of the increased bulk of the fluorenyl group relative to the Cy group and the required conformational changes to form **L2$_2$Pd**, the diphosphine complex was not formed selectively from the reaction with $Pd_2(dba)_3$. The second species showed a pair of doublets at δ_p = 55.2 and 29.0 ppm, with the former being in the region expected for the phosphonium moiety and the latter in the region previously observed for PCy_2 moiety of the LPd(dba) complex with an acyclic YPhos ligands. Thus, this species presumably is **L2**·Pd(dba), which we would expect to be a catalytically competent species according to previous studies by our as well as other groups.[16,19]

To further understanding how the ligand forms the two complexes, **L2**·Pd(dba) and **L2$_2$Pd**, we endeavored to follow the reaction of stoichiometric quantities of **L2** with $Pd_2(dba)_3$ via $^{31}P\{^{1}H\}$ NMR spectroscopy using triphenylphosphine as an internal standard. The reaction plot (Figure 8) shows that

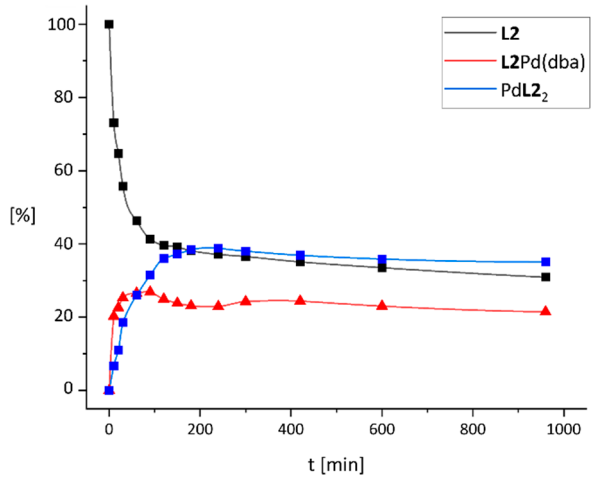

Figure 8. Schematic showing the formation of **L2**Pd(dba) and **L2$_2$**Pd complexes from free ligand **L2** and $Pd_2(dba)_3$ as monitored by $^{31}P(^{1}H)$ NMR spectroscopy with Ph3PO as internal standard.

the beginning of the reaction is characterized by the rapid formation of **L2**·Pd(dba). Within the first 30 min, the rate of formation slows considerably, while simultaneously there is an increase in the formation of **L2$_2$Pd** and a decrease in the concentration of free ligand. Within 3 h, an equilibrium state is reached. Throughout the course of the reaction, **L2$_2$Pd** is observed to slowly precipitate. These observations suggest that the combination of free ligand and **L2**·Pd(dba) leads to the formation of Pd**L**$_2$. Nonetheless, a significant amount of the proposed active catalyst **L2**·Pd(dba) remains available for entering the catalytic cycle.

Analogous to **L1**, we also synthesized palladium precatalysts **Pd$_{al}$2**, **Pd$_{cin}$2**, and **Pd$_{ind}$2**, which were obtained as pure solids in yields of 66−76% (Scheme 1). Analysis by $^{31}P\{^{1}H\}$ NMR spectroscopy showed two sets of doublets in the case of all complexes; all three had similar chemical shift and coupling constant values. These two sets of signals are probably due to the formation of diastereomers connected with the stereocenter at phosphorus and were also seen in the ^{1}H and ^{13}C NMR spectra. In the molecular structures of **Pd$_{al}$2** and **Pd$_{ind}$2**, however, only one isomer was observed (Figure 9). In contrast to the structure of **L2$_2$Pd**, the fluorenyl groups in the Pd(II) complexes remained in the desired orientation pointing toward the metal center. Nonetheless, one fluorenyl group seems not to be sufficient to fully shield one site of the metal, especially in comparison to biaryl phosphine ligands.[24] This can be seen from the steric map of **2** constructed based on the molecular structure of **Pd$_{al}$2**. Whereas the map clearly reflects the increased steric bulk of **L2** compared to **L1** exerted from both the ylide and fluorenyl substituents, the steric demand remains moderate.

Applications of **L2** in Buchwald−Hartwig aminations analogous to those described above remained unsuccessful independently of whether the active species was formed from **L2** and $Pd_2(dba)_3$ or one of the isolated precatalysts. Since the reaction monitoring of **L2** and $Pd_2(dba)_3$ has revealed that in contrast to **L1** at least some active catalyst [**L2**·Pd(dba)] should be present, we reasoned that the donor strength of **L2**

https://doi.org/10.1021/acs.organomet.1c00349
Organometallics 2021, 40, 2888−2900

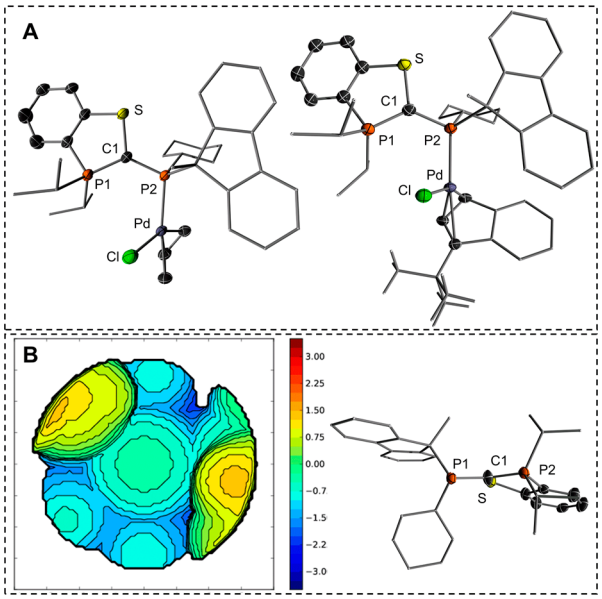

Figure 9. (Top) Molecular structures of (left) $\mathbf{Pd_{al}2}$ and (right) $\mathbf{Pd_{ind}2}$. Selected bond lengths [Å] and angles [°]: $\mathbf{Pd_{al}2}$: P1−C1 1.724(2), S1−C1 1.780(3), C1−P2 1.754(2), P2−C20 1.935(2), P2−Pd1 2.349(1), Pd1−Cl1 2.389(1), P1−C1−S1 110.3(1), P1−C1−P2 129.9(1). $\mathbf{Pd_{ind}2}$: P1−C1 1.730(2), S1−C1 1.769(2), C1−P2 1.763(2), P2−C20 1.955(2), P2−Pd1 2.319(1), Pd1−Cl1 2.373(1), P1−C1−S1 110.8(1), P1−C1−P2 131.1(1). (Bottom) Steric map of $\mathbf{Y_{Cycl}2}$ derived from the complex $\mathbf{Pd_{al}2}$ using SambVca 2.0 (P−M distance of 2.28 Å including H-atoms).[18]

would be too low to efficiently enable oxidative addition under the reaction conditions. Measurement of the CO stretching frequency in the in situ formed [**L2**·Rh(acac)(CO)] complex yielded a TEP of 2059.4 cm^{-1}. Surprisingly, this value is even higher than that of **L1**, suggesting that **L2** is an even weaker donor ligand. The high value was again confirmed by calculation of the minimum of the electrostatic potential (MESP) at the phosphorus (TEP_{ESP} = 2059.8 cm^{-1}). As both ligands display extraordinarily high TEP values and both feature the cyclic ylide moiety, we concluded that the cyclic ylide itself does not behave as a strongly electron-donating substituent.

Impact of the Cyclic Backbone on the Donor Properties. Two possible reasons can be theorized for the low electron-donating properties of the cyclic ylide: (i) the anion-stabilizing effects of the sulfur bound to the ylidic carbon or (ii) the cyclic nature of the ylide. To probe these theories further, a series of phosphines with similar cyclic ylide backbones but differing substituents **Z** in the backbone were investigated via DFT calculations and compared with related previously synthesized acyclic YPhos ligands featuring similar backbones. The MESP at the phosphine was determined, and the corresponding TEP calculated. The results are summarized in Table 1. As clearly shown by the obtained results, all cyclic phosphines examined exhibit high TEP values independent of the **Z** substituent. In contrast, the related acyclic analogues feature much lower TEP values. This observation impressively demonstrates that the presence of the sulfur atom does not play the decisive role in the observed electronic properties, but instead it is the cyclic nature of the ylide, that exerts the biggest influence on the electron-donating abilities.

To further understand the impact of the cyclic geometry on the electronic properties of the YPhos ligands, we analyzed the

Table 1. Calculated TEP Values of YPhos Ligands with Cyclic Ylide Backbones and Comparable Acyclic YPhos Ligands Previously Reported

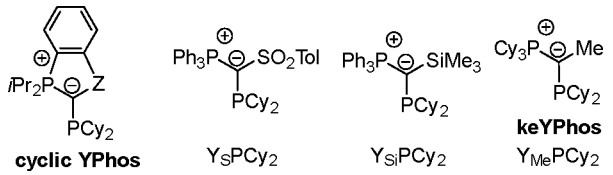

cyclic YPhos | Y_SPCy_2 | $Y_{Si}PCy_2$ | keYPhos $Y_{Me}PCy_2$

Z (cyclic YPhos)	MESP [eV]	TEP_{ESP} [cm^{-1}]	acyclic YPhos ligand	TEP_{exp} [cm^{-1}]
S	−54.15914	2057.1		
SO	−54.14821	2060.3		
SO_2	−54.14466	2061.3	Y_SPCy_2[13]	2055.1
NMe	−54.15479	2058.4		
$SiMe_2$	−54.15951	2057.0	$Y_{Si}PCy_2$[13]	2048.8
CMe_2	−54.16339	2055.9	$Y_{Me}PCy_2$[14a]	2050.1

electronic structure of the ligands by natural bond orbital (NBO) analyses (Table 2). These NBO studies reinforced our assumption by showing significant changes in the character of the P−C bond. Thus, the orbital of the ylidic carbon atom involved in the P−C bond to the phosphine moiety of **L1** and **L2** features a higher s-character in comparison to what would be expected for an ideal sp^2-hybridized carbon center (values of 39.4 vs 33.3%). This increased s-character is due to the small P−C−S angle of 111.4° which is enforced by the geometric restraints of the ring structure and results in a higher p-character in the corresponding bonds. For comparison reason, the electron-rich, acyclic keYPhos and joYPhos ligands were also investigated. As expected, keyPhos showed a much lower s-character in the P−C bond due to the larger P−C−C_{Me} angle of 117.2°, and joYPhos, which is most electron-rich donor in this series, features the largest angle of 123.0° and thus displays the lowest s-character within the orbital with only 30.8%. As a result of this high s-character within the bonding orbital of **L1**, the C−P bond is much more polarized toward the carbon atom, thus explaining why the cyclic ylide in **L1** and **L2** donates less electron density toward the phosphine. This explanation is also in agreement with the observation that keYPhos and joYPhos are much more electron-rich, with these species having a lower s-character and hence a less polarized C−P bond. This observation impressively demonstrates that the angle between the phosphonium moiety, the ylidic carbon atom, and **Z** substituent has a significant influence on the overall donor ability of the ligand system. It is noteworthy that studies on the angle dependency of metal ligand interactions have been reported before, particularly focusing on the impact of the angle at the donor site (i.e., the C−P−C angles) on the donor properties.[24]

To obtain a quantitative estimation of the impact of the cyclic structure on the donor properties, cyclic ligand **L3** with **Z** = SO_2 was calculated and compared to its acyclic counterpart Y_SPCy_2. Similar to the observations mentioned above, the acyclic ligand features a much larger P−C−S angle, resulting in a higher p-character on the σ(C) orbital and therefore in a higher bond polarization toward the phosphorus atom and a lower TEP value.

We further evaluated the angle-dependency of the donor strength by computationally increasing the angle at the ylidic carbon atom on the example of the acyclic YPhos ligand, keYPhos and monitoring the impact on the electronic structure

https://doi.org/10.1021/acs.organomet.1c00349
Organometallics 2021, 40, 2888−2900

Table 2. Results of the NBO Analysis of YPhos Ligands, Observed P−C−Z Angles, and Their Measured TEP Values[a]

ligand	α-P−C−Z angle [deg]	σ(C) s-character	σ(C) p-character	bond polarization % P	bond polarization % C	TEP [cm^{-1}]
L1	111.44	39.4%	60.5%	34.8%	65.2%	2057.1
keYPhos	117.17	33.5%	66.4%	36.5%	63.5%	2050.1
joYPhos	122.98	30.8%	69.1%	41.2%	58.8%	2049.3
L3	111.14	38.2%	61.8%	33.6%	66.3%	2061.3[b]
Y_SPCy_2[b]	121.50	36.5%	63.5%	34.9%	65.1%	2057.0

[a]

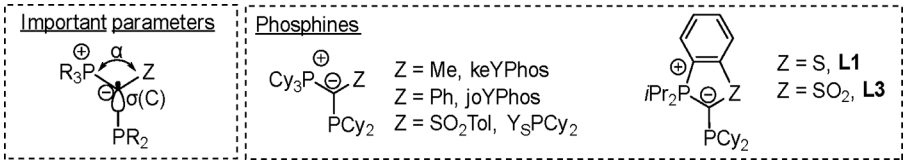

[b]Calculated TEP from MESP.

(Figure 10). Increasing the Cy_3P-C-C_{Me} angle from 90 to 120° resulted in an increase of s-character in the respective

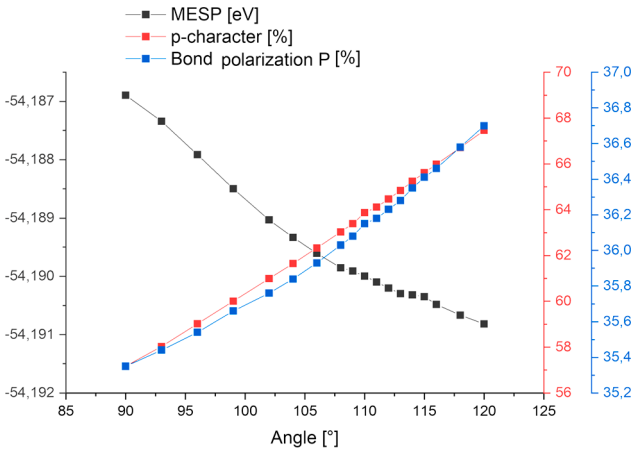

Figure 10. Calculated MESP values at the lone pair at the phosphorus, p-character of σ(C), and polarization of the C−PCy_2 bond toward the P atom depending on the P−C−C angle in the keYPhos ligand.

bonds and hence in an increase of p-character of σ(C) in the P−C bond to the phosphine moiety. This simultaneously leads to a lower bond polarization toward the carbon atom and hence to a lower (more negative) MESP value. Overall, the widening of the P−C−C-angle in keYPhos by 30° leads to a decrease of the TEP value by 1.4 cm^{-1}. This change is similar to the expected change when replacing one *n*-butyl group (χ_i = 1.4 cm^{-1}) such as in P(*n*-Bu)$_3$ by a *tert*-butyl substituent (χ_i = 0 cm^{-1}).[6b]

CONCLUSION

In summary, we have reported on the synthesis and characterization of two novel YPhos ligands with a cyclic ylide and a PCy_2 (**L1**) and P(Cy)(Flu^{Me}) substituent (**L2**, Flu^{Me} = 9-methylfluorenyl), respectively. The unexpected complete inactivity of various palladium complexes of these ligands in Buchwald−Hartwig aminations led us to a detailed investigation of the spatial and electronic properties of the novel phosphines. Analysis from a spatial viewpoint revealed that the cyclic ylide offers very little steric protection toward the metal center in complexes with **L1**, thus leading to the facile formation of the corresponding catalytically inactive L_2Pd species. Formation of this bisphosphine complex can be hampered by the bulkier fluorenyl substituent in **L2**, but this still does not allow for any catalytic activity. Experimental determination of the donor strength revealed a remarkably decreased donor capacity of **L1** and **L2** compared with previously reported YPhos ligands featuring acyclic ylide substituents. Computational studies showed that the decreased donor strength results from the cyclic backbone. The tight P−C−S bond angle in the cyclic ylide increases the s-character of the bonding orbital of the ylidic carbon atom in the C−P bond, thus resulting in a strong polarization of the C−P bond toward the carbon and hence in a decreased electron density at the phosphorus atom. Overall, these results demonstrate a marked angle-dependency of the donor strength of ylide-substituted phosphines, which may be used as further tool in the design of new YPhos ligands in the future.

EXPERIMENTAL SECTION

General Procedures. All experiments unless otherwise stated were performed under a dry, oxygen-free argon atmosphere using standard Schlenk techniques. Solvents involved were dried with an MBraun solvent-purification system (SPS 800) or with standard methods and stored under an argon atmosphere over 3 or 4 Å molecular sieves. ^{1}H, ^{13}C{^{1}H}, and ^{31}P{^{1}H} NMR spectra were recorded on an Avance III 400 spectrometer from Bruker at 25 °C. Chemical shifts are given in ppm regarding the δ scale and are referenced to the residual protons of the deuterated solvent. All spin−spin coupling constants are given in Hz. Multiplicities are indicated with the following abbreviations: s = singlet, d = doublet, t = triplet, q = quartet, dt = doublet of triplets, and so on. The assignment of signals was supported by HSQC, HMBC, APT, and COSY experiments. Elemental analyses were performed by Manuela Winter and Dr. Harish Parala on an Elementar vario MICRO-cube from Elementar. All chemicals were obtained from commercial sources and used without further purification. Dicyclohexylchlorophosphine and (tht)AuCl were made according to literature methods.[25,26]

Synthesis of [1]I.

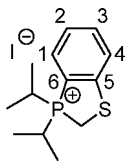

In a flask fitted with an addition funnel, 60 mL (99.8 mmol) of a 1.66 M *n*BuLi solution in hexane was added to 50 mL of cyclohexane. An additional 30 mL of cyclohexane and 15 mL (11.6 g, 99.8 mmol) of TMEDA were added afterward slowly, followed by a further 20 mL of cyclohexane. The solution was cooled to 0 °C and 4.66 mL (5 g, 45.4

https://doi.org/10.1021/acs.organomet.1c00349
Organometallics 2021, 40, 2888−2900

mmol) of thiophenol dissolved in 10 mL of cyclohexane was added slowly. The solution was stirred for 30 min at 0 °C, warmed to room temperature, and stirred overnight. A colorless solid precipitated that was subsequently filtered off and washed with three 30 mL portions of hexane. The solid was dried *in vacuo* (10.0 g, 44.8 mmol). The dilithiated product was dissolved in 100 mL of THF and cooled to −80 °C. Next, 7.15 mL (6.84 g, 44.8 mmol) of diisopropylchlorophosphine was slowly added via an addition funnel at −80 °C over a period of 1 h. The solution was stirred and allowed to warm to room temperature overnight. The solvent was removed, and the remaining solid was dried *in vacuo* (15 g, 38.4 mmol). The obtained solid was dissolved in 200 mL of diethyl ether and 3.09 mL (10.2 g, 38.4 mmol) of diiodomethane was added slowly before being left to stir overnight. The solvent was removed, and the residue redissolved in 50 mL of DCM. The undissolved salts were filtered off. The solvent was removed, and the remaining solid was suspended in 50 mL of THF, filtered, and washed (2 × 20 mL) with THF. The colorless solid was dried *in vacuo*. Phosphonium salt [**1**]I could be obtained as a colorless solid (9.4 g, 25.7 mmol, 56.5% yield). ^{1}H NMR (400 MHz, DCM-d_2): δ [ppm] = 1.33 (d, 3H, ^{3}J = 7.15 Hz, *i*Pr CH_3), 1.38 (d, 3H, ^{3}J = 7.15 Hz, *i*Pr CH_3), 1.41 (d, 3H, ^{3}J = 7.12 Hz, *i*Pr CH_3), 1.46 (d, 3H, ^{3}J = 7.12 Hz, *i*Pr CH_3), 3.61 (ds, 2H, ^{3}J = 7.15, 7.15, 7.12, 7.12 Hz, $^{2}J_{HP}$ = 10.57 Hz, *i*Pr CH(CH$_3$)$_2$), 4.30 (d, 2H, ^{2}J = 9.45 Hz, PCHS), 7.43 (m, 1H, CH Pos. 4), 7.49 (m, 1H, CH Pos. 2), 7.68 (m, 1H, CH Pos. 1), 7.89 (m, 1H, CH Pos. 3). ^{13}C{^{1}H} NMR (100.6 MHz, DCM-d_2): δ [ppm] = 16.2 (d, $^{2}J_{CP}$ = 15.2 Hz, *i*Pr CH_3), 16.3 (d, $^{2}J_{CP}$ = 15.2 Hz, *i*Pr CH_3), 17.5 (d, $^{1}J_{CP}$ = 42.7 Hz, PCH_2S), 23.9 (d, $^{1}J_{CP}$ = 40.4, *i*Pr CH(CH$_3$)$_2$), 113.2 (d, $^{1}J_{CP}$ = 85.6, *C* Pos. 6), 124.8 (d, $^{3}J_{CP}$ = 9.2 Hz, CH Pos. 2/4), 126.9 (d, $^{3}J_{CP}$ = 10.3 Hz, CH Pos. 2/4), 132.4 (d, $^{2}J_{CP}$ = 10.6 Hz, CH Pos. 1), 136.1 (d, $^{4}J_{CP}$ = 2.6 Hz, CH Pos. 3), 150.3 (d, $^{2}J_{CP}$ = 16.9 Hz, *C*H Pos. 5). ^{31}P{^{1}H} NMR (162.1 MHz, DCM-d_2): δ [ppm] = 76.5 (s, *P*CS). IR (ATR) [cm^{-1}]: 3051 (w), 2979 (w), 2859 (m), 1574 (s), 1452 (s), 1427 (s), 1271 (m), 1140 (s), 1116 (m), 1036 (w), 884 (m), 783 (s), 145 (m), 676 (s), 632 (m), 482 (s), 461 (s), 450 (s), 430 (m). CHNS for $C_{13}H_{20}IPS$: Calcd: C: 42.63, H: 5.50, S: 8.75. Measured: C: 42.57, H: 5.38, S: 8.43. Melting point: 160.1 °C.

Synthesis of ***2***. In a Schlenk tube, 2.50 g (6.83 mmol) of phosphonium salt [**1**]I and 930.0 mg (8.29 mmol) of KO*t*-Bu were suspended in 15 mL of THF. The suspension immediately turned orange. The suspension was stirred for 2 h at room temperature before removal of the solvent under reduced pressure, with the residue redissolved in 10 mL of pentane and stirred for 15 min. The solution was filtered, and the white residue was washed (2 × 5 mL) with pentane. The solvent of the combined solutions was removed and 1.55 g (6.47 mmol, 95%) of ylide **2** was obtained as a dark red liquid. ^{1}H NMR (400 MHz, C_6D_6): δ [ppm] = 0.76 (d, 3H, ^{3}J = 7.06 Hz, *i*Pr CH_3), 0.79 (d, 3H, ^{3}J = 6.76 Hz, *i*Pr CH_3), 0.83 (d, 3H, ^{3}J = 6.76 Hz, *i*Pr CH_3), 0.86 (d, 3H, ^{3}J = 7.11 Hz, *i*Pr CH_3), 1.42 (d, 1H, $^{2}J_{HP}$ = 23.0 Hz, PCHS), 1.81 (dq, 1H, ^{3}J = 7.12, 7.12, 7.12 Hz, $^{2}J_{HP}$ = 14.2 Hz, *i*Pr CH(CH$_3$)$_2$), 6.83 (m, 1H, CH Pos. 4), 6.94 (m, 1H, CH Pos. 2), 7.14(m, 1H, CH Pos. 1), 7.40 (m, 1H, CH Pos. 3). ^{13}C{^{1}H} NMR (100.6 MHz, C_6D_6): δ [ppm] = −3.4 (d, $^{1}J_{CP}$ = 103.0 Hz, PCHS), 16.5 (dd, $^{2}J_{CP}$ = 154.2 Hz, ^{2}J = 2.42 Hz, *i*Pr CH_3), 29.1 (d, $^{1}J_{CP}$ = 48.6, *i*Pr CH(CH$_3$)$_2$), 115.2 (d, $^{1}J_{CP}$ = 94.8, *C* Pos. 6), 121.4 (d, $^{4}J_{CP}$ = 9.6 Hz, CH Pos. 4), 124.2 (d, $^{4}J_{CP}$ = 7.48 Hz, CH Pos. 2), 127.8 (d, $^{4}J_{CP}$ = 2.35 Hz, CH Pos. 3), 129.2 (d, $^{2}J_{CP}$ = 9.84 Hz, CH Pos. 1), 153.6 (d, $^{2}J_{CP}$ = 21.4 Hz, CH Pos. 5). ^{31}P{^{1}H} NMR (162.1 MHz, C_6D_6): δ [ppm] = 50.2 (s, *P*CS).

Synthesis of ***L1***. First, 1.55 g (6.47 mmol) of ylide **2** was dissolved in 15 mL of THF and cooled to 0 °C. To this, 0.79 mL (865.8 mg, 3.56 mmol) of PCy_2Cl was slowly added over 10 min. Upon addition of the chlorophosphine, the phosphonium salt precipitated as a colorless solid. It was stirred for 2 h at room temperature and filtered, and the solid was washed with (2 × 5 mL) THF. The solvent was removed under reduced pressure, and the red-orange residue was suspended in 5 mL of acetonitrile and stirred for 15 h. Overnight, an orange solid precipitated that was filtered off, washed (2 × 5 mL) with acetonitrile, and dried *in vacuo*. Ylide-substituted phosphine **L1** was obtained in 79% yield (2.54 mmol, 1.1 g). ^{1}H NMR (400 MHz, THF-d_8): δ [ppm] = 1.12 (d, 3H, ^{3}J = 7.12 Hz, *i*Pr CH_3), 1.16 (d, 3H, ^{3}J = 7.12 Hz, *i*Pr CH_3), 1.21 (d, 3H, ^{3}J = 7.12 Hz, *i*Pr CH_3), 1.25 (d, 3H, ^{3}J = 7.12 Hz, *i*Pr CH_3), 1.20−1.35 (m, 10H, PCy_2 H_{2+3+4}), 1.70−1.85 (m, 2H, PCy_2 H_{2+3+4}), 1.92 (m, 2H, PCy_2 H_1), 2.49 (dp, 2H, ^{3}J = 7.12, 7.12, 7.12, 7.12 Hz, $^{1}J_{HP}$ = 10.1 Hz, *i*Pr CH(CH$_3$)$_2$), 7.03 (m, 1H, CH Pos. 4), 7.20 (m, 1H, CH Pos. 2), 7.29 (m, 1H, CH Pos. 1), 7.48 (m, 1H, CH Pos. 3). ^{13}C{^{1}H} NMR (100.6 MHz, THF-d_8): δ [ppm] = 5.7 (dd, $^{1}J_{CP}$ = 34.7, 105.32 Hz, PCS), 16.75 (dd, $^{2}J_{CP}$ = 1.99 Hz, *i*Pr CH_3), 17.8 (d, $^{2}J_{CP}$ = 2.22 Hz, *i*Pr CH_3), 28.0 (s, CH_2 PCy_2 $C_{3/4}$), 28.7 (m, CH_2 PCy_2 $C_{3/4}$), 30.3 (d, $^{1}J_{CP}$ = 49.36 Hz, *i*Pr CH(CH$_3$)$_2$), 31.5 (m, CH_2 PCy_2 $C_{3/4}$), 32.8 (d, $^{2}J_{CP}$ = 18.7 Hz, CH_2 PCy_2 C_2), 36.6 (dd, ^{2}J = 4.8 Hz, $^{2}J_{CP}$ = 9.43, CH_2 PCy_2 C_1), 118.4 (d, $^{1}J_{CP}$ = 91.0 Hz, *C* Pos. 6), 122.8 (d, $^{4}J_{CP}$ = 9.2, CH Pos. 3), 123.8 (d, $^{3}J_{CP}$ = 6.9, CH Pos. 2/4), 129.5 (d, $^{3}J_{CP}$ = 1.3 Hz, CH Pos. 2/4), 129.9 (d, $^{2}J_{CP}$ = 2.6 Hz, CH Pos. 1), 155.7 (dd, $^{2}J_{CP}$ = 18.9 Hz, *C* Pos. 5). ^{31}P{^{1}H} NMR (162.1 MHz, THF-d_8): δ [ppm] = −14.9 (d, $^{2}J_{PP}$ = 108.6 Hz, PCy_2), 50.67 (d, $^{2}J_{PP}$ = 108.6 Hz, *P*CS). IR (ATR) [cm^{-1}]: 2917 (s), 2851 (m), 1439 (m), 1108 (s), 1048 (m), 874 (m), 849 (w), 711 (m), 690 (s), 653 (m), 538 (w), 471 (m), 450 (w). CHNS for $C_{25}H_{40}P_2S$: Calcd: C: 69.09, H: 9.28, S: 7.38. Measured: C: 68.89, H: 9.14, S: 7.38. Melting point: 93.7 °C.

Synthesis of ***L1·AuCl***. A Schlenk tube was charged with **L1** (200 mg, 459 μmol, 1 equiv), (tht)AuCl (147 mg, 459 μmol, 1 equiv), and 4 mL of THF, and the mixture was stirred overnight. The solvent was removed *in vacuo*, and the residue dissolved in 2 mL of DCM. The solution was layered with 20 mL of pentane and left for 1 day. A yellow solid precipitated. The solution was then cooled to −30 °C for 2 more days. The solid was filtered off and washed (2 × 5 mL) with pentane. 224 mg (336 μmol, 73%) of the yellow crystalline solid was obtained. Slow diffusion of pentane into a solution of **L1·AuCl** in C_6D_6 allowed crystals suitable for single-crystal XRD to be obtained. ^{1}H NMR (400 MHz, CD_2Cl_2): δ [ppm] = 1.14−1.34 (4 ×rd, 12 H, $^{3}J_{PH}$ = 7.0 Hz, *i*Pr CH_3), 1.14−1.34 (m, 6H, PCy_2 CH_2), 1.34−1.57 (m, 6H, PCy_2 CH_2), 1.63−1.71 (m, 2H, PCy_2 CH_2), 1.77−1.88 (m, 4H, PCy_2 CH_2), 1.95−2.06 (m, 4H, PCy_2 CH_2), 2.15 (tdd, 2H, $^{2}J_{HP}$ = 12.1 Hz, ^{3}J = 7.0, 3.3 Hz), 3.13 (dp, 2H, $^{2}J_{HP}$ = 8.9 Hz, ^{3}J = 7.1, 7.1, 7.0, 7.0, *i*Pr CH), 7.12−7.18 (m, 1H, Pos. 4), 7.30−7.39 (m, 2H, Pos. 2 + Pos. 3), 7.46−7.51 (m, 1H, Pos. 1). ^{13}C{^{1}H} NMR (101 MHz, CD_2Cl_2): δ [ppm] = 0.8 (dd, $^{1}J_{CP}$ = 103.9, 66.1 Hz, PCS), 17.0 (dd, $^{2}J_{CP}$ = 42.6 Hz, ^{2}J = 2.0 Hz, *i*Pr CH_3), 26.6 (d, ^{2}J = 1.7 Hz, PCy_2 CH_2), 27.1−27.5 (m, PCy_2 CH_2), 29.2 (d,$^{1}J_{CP}$ = 48.9 Hz, *i*Pr CH), 30.3 (d, ^{2}J = 1.9 Hz, PCy_2 CH_2), 32.0 (d, ^{2}J = 2.8 Hz, PCy_2 CH_2), 37.7 (dd, $^{1}J_{CP}$ = 41.5 Hz, ^{2}J = 1.8 Hz, PCy_2 CH), 118.2 (dd, $^{1}J_{CP}$ = 92.7 Hz, ^{2}J = 6.7 Hz, *C* Pos. 6), 122.9 (d, $^{3}J_{CP}$ = 7.1 Hz, CH Pos. 2), 123.7 (d, $^{3}J_{CP}$ = 9.6 Hz, CH Pos. 4), 129.6 (d, $^{2}J_{CP}$ = 10.1 Hz, CH Pos. 1), 130.8 (d, ^{3}J = 2.2 Hz, CH Pos. 3), 151.5 (dd, $^{2}J_{CP}$ = 15.8 Hz, ^{2}J = 5.1 Hz, *C* Pos. 5). ^{31}P{^{1}H} NMR (162.1 MHz, CD_2Cl_2): δ [ppm] = 27.1 (d, $^{2}J_{PP}$ = 51.8 Hz, PCy_2), 57.2 (d, $^{2}J_{PP}$ = 50.5 Hz, *P*CS). IR (ATR) [cm^{-1}]: 2919 (m), 1444 (m), 1110 (m), 1066 (s), 897 (m), 741 (s), 711 (s), 687 (m), 667 (m), 636 (w), 520 (m), 445 (m), 408 (m). CHNS for $C_{25}H_{40}AuClP_2S$: Calcd: C: 45.02, H: 6.04, S: 4.81. Measured: C: 44.79, H: 6.10, S: 4.43. Melting point: 207.3 °C (decomposition).

Synthesis of ***L1$_2$Pd***. A Schlenk tube charged with **L1** (200 mg, 460 μmol, 1 equiv), Pd_2dba_3 (155 mg, 230 μmol, 1 equiv), and 4 mL of THF was stirred at room temperature for 1 h. The solution was subsequently filtered, over-laid with 10 mL of pentane, and left for 3 days. A yellow solid precipitated from the solution. The solid was filtered off and washed (2 × 5 mL) with THF; 181 mg (185 μmol, 81%) of the yellow solid was obtained. Slow diffusion of pentane into a solution of **L1$_2$Pd** in C_6D_6 allowed for crystals suitable for single-crystal XRD to be obtained. ^{1}H NMR (400 MHz, THF-d_8): δ [ppm] = 1.12 (dd, 6H, ^{3}J = 7.16, 16.71 Hz, *i*Pr CH_3), 1.41 (dd, 6H, ^{3}J = 7.16, 16.71 Hz, *i*Pr CH_3), 1.3−1.5 (m, 6H, PCy2 $H_{1+2+3+4}$), 1.76 (m, 2H, PCy2 $H_{1+2+3+4}$), 1.8−2.0 (m, 8 H, PCy_2 H_{2+3+4}), 2.1−2.4 (m, 6H, PCy_2 H_{2+3+4}), 3.72 (dp, 2H, ^{3}J = 7.05, 7.05, 7.05, 7.05 Hz, $^{2}J_{HP}$ = 10.1 Hz, *i*Pr CH(CH$_3$)$_2$), 6.72 (m, 1H, CH Pos. 4), 6.88 (m, 1H, CH Pos. 2), 6.92 (m, 1H, CH Pos. 1), 7.02 (m, 1H, CH Pos. 3). ^{13}C{^{1}H}

https://doi.org/10.1021/acs.organomet.1c00349
Organometallics 2021, 40, 2888−2900

NMR: Not possible due to poor solubility of the pure compound in deuterated solvent. $^{31}P\{^{1}H\}$ NMR (162.1 MHz, THF-d_8): δ [ppm] = 13.11 (dd, $^{2}J_{PP}$ = 44.9, 34.2 Hz PCy_2), 50.7 (dd, $^{2}J_{PP}$ = 45.0, 34.2 Hz, *P*CS). IR (ATR) [cm^{-1}]: 2914 (m), 2843 (m), 1441 (m), 1257 (w), 1109 (m), 1058 (s), 1000 (w), 887 (m), 868 (s), 851 (w), 741 (s), 712 (m), 366 (m), 543 (w), 514 (m), 471 (m), 441 (m), 406 (m). CHNS for $C_{50}H_{80}P_4PdS_2$: Calcd: C: 61.56, H: 8.27, S: 6.57. Measured: C: 61.88, H: 7.87, S: 6.49. Melting point: 195.8 °C (decomposition).

Synthesis of ***Pd$_{al}$1***. 250 mg (0.58 mmol) of **L1** and 108 mg of $[Pd(allyl)Cl]_2$ (56.4 m% Pd, 0.29 mmol) were suspended in 10 mL of pentane and stirred for 30 min. A yellow suspension formed, which was filtered, and the remaining solid was washed (2 × 5 mL) with pentane. Complex **Pd$_{al}$1**was obtained as a yellow solid in 74% yield (255 mg, 0.56 mmol). By slow diffusion of pentane into a solution of **Pd$_{al}$1**in C_6D_6 crystals of a decomposition product suitable for single-crystal XRD could be obtained. ^{1}H NMR (400 MHz, C_6D_6): δ [ppm] = 0.88−1.10 (m, 6H, *i*Pr CH_3), 1.10−1.29 (m, 8H, *i*Pr CH_3, PCy_2 CH_2 H_{2+3+4}), 1.30−1.92 (m, 13H, PCy_2 CH_2 H_{2+3+4}), 2.21−2.31 (d, 2H, J^3 = 12.5 Hz, PCy_2 CH_2 H_{2+3+4}), 2.32 (d, 2H, J^3 = 11.2 Hz, Allyl CH_2 H_5), 2.38−2.53 (dt, 2H, J^3 = 9.0, 9.0, 22.2 Hz, PCy_2 CH_2 H_{2+3+4}), 2.53−2.71 (p, 2H, J^3 = 15.1, 15.1, 17.1, 17.1 Hz, PCy_2 CH_2 H_1), 3.47 (dd, 1H, J^3 = 8.7, 13.8 Hz, Allyl CH_2 H_2), 5.53 (m, 1H, Allyl CH_2 H_4), 3.6 (dp, 1H, J^3 = 5.24, 5.24, 5.25, 5.25 Hz, J^2_{HP} = 14.2 Hz, *i*Pr C*H*), 3.74 (dp, 1H, J^3 = 7.04, 7.04, 7.05, 7.05 Hz, J^2_{HP} = 14.2 Hz, *i*Pr C*H*), 4.52 (t, 1H, J^3 = 7.19, 7.19 Hz, Allyl CH H_3), 4.89 (ddd, 1H, J^3 = 7.96, 13.7, 17.9 Hz, Allyl CH H_1), 6.83−6.91 (m, 1H, C*H* Pos. 4), 6.83−6.91 (m, 1H, C*H* Pos. 2), 7.01−7.12 (m, 1H, C*H* Pos. 1), 7.13−7.23 (m, 1H, C*H* Pos. 3). $^{13}C\{^{1}H\}$ NMR (101 MHz, C_6D_6) δ [ppm] = 6.01 (dd, $^{1}J_{CP}$ = 37.9, 106.5 Hz, PCS), 18.1 (d, *J* = 2.2 Hz, *i*Pr CH_3), 26.9 (s, CH_2 PCy_2 C_{2+3+4}), 27.7 (d, ^{2}J = 12.1 Hz, CH_2 PCy_2 C_{2+3+4}), 28.1 (d, ^{2}J = 12.6 Hz, CH_2 PCy_2 C_{2+3+4}), 30.0 (s, CH_2 PCy_2 C_{2+3+4}), 30.1 (s, CH_2 PCy_2 C_{2+3+4}), 30.4(s, CH_2 PCy_2 C_{2+3+4}), 30.6 (d, $^{1}J_{CP}$ = 6.5 Hz, *i*Pr $CH(CH_3)_2$), 40.4 (dd, $^{1}J_{CP}$ = 74.1 Hz, ^{2}J = 26.7 Hz, *C*H PCy_2 C_1), 50.7 (d, ^{2}J = 2.3 Hz, CH_2 allyl), 79.6 (d, ^{2}J = 29.1 Hz, CH_2 allyl), 114.3 (d, ^{2}J = 4.6 Hz, *C*H allyl), 118.0 (dd, $^{1}J_{CP}$ = 90.0 Hz,^{2}J = 5.9 Hz, Pos. 6), 122.2 (d, ^{2}J = 9.2 Hz, Pos. 4), 122.9 (d, ^{2}J = 6.7 Hz, Pos. 3), 129.5 (d, ^{2}J = 2.2 Hz, Pos. 2), 130.2 (d, ^{2}J = 9.3 Hz, Pos. 1), 152.8 (dd, ^{2}J = 15.5 Hz, ^{2}J = 3.1 Hz, Pos. 5). $^{31}P\{^{1}H\}$ NMR (162.1 MHz, C_6D_6): δ [ppm] = 20.3 (d, $^{2}J_{PP}$ = 60.8 Hz, PCy_2), 55.5 (d, $^{2}J_{PP}$ = 61.1 Hz, *P*CS). IR (ATR) [cm^{-1}]: 2924 (m), 2845 (w), 1442 (m), 1262 (w), 1106 (m), 1064 (s), 864 (m), 742 (s), 657 (m), 459 (m), 405 (w). CHNS for $C_{28}H_{45}ClP_2PdS$: Calcd: C: 54.37, H: 7.50, S: 5.18. Measured: C: 54.22, H: 7.79, S: 5.18. Melting point: 146.7 °C (decomposition).

Synthesis of ***Pd$_{cin}$1***. First, 200 mg (0.46 mmol) of **L1** and 118 mg of $[Pd(Cinnamyl)Cl]_2$ (40.2 m% Pd, 0.23 mmol) were suspended in 8 mL of pentane and stirred for 2 h. A red suspension formed. This was filtered, and the solid was washed (2 × 5 mL) with pentane. Complex **Pd$_{cin}$1** was obtained as a red-orange solid in 55.2% yield (176 mg, 0.25 mmol). By slow diffusion of pentane into a solution in THF-d_8, crystals suitable for X-ray diffraction could be obtained. ^{1}H NMR (400 MHz, THF-d_8): δ [ppm] = 1.07−1.85 (m, 27H, *i*Pr CH_3 + PCy_2 CH_2 H_{2+3+4}), 1.97−2.26 (m, 5H, PCy_2 CH_2 H_{2+3+4}), 2.30−2.52 (m, 2H, PCy_2 CH H_1), 2.69−2.77 (d, 1H, ^{3}J = 11.9 Hz, cin CH_2), 3.58 (m, 1H, *i*Pr C*H*), 3.71 (m, 1H, *i*Pr C*H*), 3.80 (d, 1H, ^{3}J = 6.7 Hz, *i*Pr C*H*), 5.06 (dd, 1H, ^{3}J = 13.1, 9.3 Hz, cin C*H*), 5.83 (m, 1H, cin C*H*Ph), 7.02−7.10 (m, 1H, Pos. 4), 7.19−7.29 (m, 4H, cin C*H* Ph + Pos. 2), 7.31−7.37 (m, 1H, Pos. 1), 7.42−7.46 (m, 2H, cin C*H* Ph), 7.49−7.55 (m, 1H, Pos.3). ^{13}C NMR (101 MHz, THF-d_8): δ [ppm] = 7.2 (dd, $^{1}J_{CP}$ = 107.2, 39.1 Hz, PCS), 18.6 (d, $^{2}J_{CP}$ = 2.2 Hz, *i*Pr CH_3), 18.8 (d, $^{2}J_{CP}$ = 2.0 Hz, *i*Pr CH_3), 23.4 (s, PCy_2 CH_2), 27.6 (s, PCy_2 CH_2), 28.0−31.3 (m, PCy_2 CH_2), 32.0 (d, $^{1}J_{CP}$ = 46.4 Hz, *i*Pr CH), 40.0 (d, $^{1}J_{CP}$ = 27.2 Hz, PCy_2 *C*H), 42.5 (d, $^{1}J_{CP}$ = 25.6 Hz, PCy_2 *C*H), 48.1 (d, ^{2}J = 2.6 Hz, cin CH_2), 98.8 (d, ^{2}J = 26.8 Hz, cin CH), 109.6 (d, ^{2}J = 5.2 Hz, cin CHPh), 118.7 (dd, $^{1}J_{CP}$ = 89.7 Hz, ^{2}J = 5.6 Hz, Pos. 6), 123.0 (d, $^{3}J_{CP}$ = 9.2 Hz, Pos. 4), 123.4 (d, $^{3}J_{CP}$ = 6.7 Hz, Pos.2), 127.9 (d, $^{2}J_{CP}$ = 2.4 Hz, Pos. 1), 128.7 (d, ^{2}J = 3.3 Hz, cin CH Ph), 129.1 (d, ^{2}J = 2.0 Hz, cin *C*H Ph), 130.2 (d, ^{2}J = 2.2 Hz, cin CH Ph), 131.5 (d, ^{2}J = 9.5 Hz, Pos. 3), 138.7 (d, ^{2}J = 6.1 Hz, cin *C* Ph), 153.5 (dd, $^{2}J_{CP}$ = 15.3 Hz, ^{2}J = 3.1 Hz, Pos. 5). ^{31}P NMR (162 MHz, THF-d_8) δ = 24.8 (d, $^{2}J_{PP}$ = 61.3 Hz, PCy_2), 55.53 (d, $^{2}J_{PP}$ = 60.9 Hz, *P*CS). IR (ATR) [cm^{-1}]: 2918 (m), 1442 (m), 1107 (m), 1059 (s), 872 (m), 741 (s), 688 (s), 657 (w), 513 (w), 458 (m), 411 (m). CHNS for $C_{34}H_{49}ClP_2PdS$: Calcd: C: 58.87, H: 7.12, S: 4.62. Measured: C: 59.18, H: 7.22, S: 4.39. Melting point: 115.2 °C (decomposition).

Synthesis of ***Pd$_{in}$1***. First, 250 mg (0.58 mmol) of **L1** and 178 mg of $[Pd(^{t}Bu\text{-}Indenyl)Cl]_2$ (33.2 m% Pd, 0.29 mmol) were suspended in 10 mL of pentane and stirred for 2 h. The dark gray suspension formed was filtered, and the solid was washed (2 × 5 mL) with pentane. Complex **Pd$_{in}$1** was obtained as a gray solid in 84.2% yield (352 mg, 0.47 mmol). By slow diffusion of pentane into a solution of **Pd$_{in}$1** in C_6D_6, crystals suitable for single-crystal XRD could be obtained. ^{1}H NMR (400 MHz, C_6D_6): δ [ppm] = 0.84−0.98 (m, 4H, *i*Pr CH_3), 1.02−1.13 (m, 6H, *i*Pr CH_3), 1.18 (m, 2H, *i*Pr CH_3), 1.22−1.88 (m, 18H, PCy_2 CH_2 H_{2+3+4}), 1.68 (s, 9H, ^{t}Bu CH_3), 2.21 (m, 3H, PCy_2 CH_2 H_{2+3+4}), 2.42 (m, 1H, PCy_2 CH_2 H_{2+3+4}), 2.60 (dqd, 2H, ^{3}J = 3.17, 9.35, 9.47, 12.1 Hz, PCy_2 CH H_1), 3.55 (dp, 1H, $^{2}J_{PH}$ = 14.2 Hz, ^{3}J = 7.2, 7.2, 7.24, 7.24 Hz, *i*Pr C*H*), 4.18 (dp, 1H, $^{2}J_{PH}$ = 14.2 Hz, ^{3}J = 7.2, 7.2, 7.24, 7.24 Hz, *i*Pr C*H*), 5.43 (dd, 1H, ^{2}J = 1.37, 2.89 Hz, Ind), 6.32 (dd, 1H, ^{2}J = 0.92, 2.93 Hz, C*H*, Ind), 6.71 (m, 1H, C*H* Pos. 4), 6.79 (m, 1H, C*H*, Ind), 6.85 (m, 1H, C*H* Pos. 2), 6.93 (m, 1H, C*H*, Ind), 7.03 (m, 2H, C*H* Pos 1 + Ind), 7.19 (m, 1H, C*H* Pos 3), 7.47 (m, 1H, C*H*, Ind). $^{13}C\{^{1}H\}$ NMR (101 MHz, C_6D_6) δ = 7.24 (dd, ^{2}J = 106.6, 42.8 Hz, PCS), 17.9 (d, ^{2}J = 1.9 Hz, *i*Pr CH_3), 18.1 (d, ^{2}J = 2.2 Hz, *i*Pr CH_3), 18.2 (d, ^{2}J = 2.1 Hz, *i*Pr CH_3), 18.6 (d, ^{2}J = 2.2 Hz, *i*Pr CH_3), 26.5 (d, ^{2}J = 20.5 Hz, CH_2 PCy_2 C_{2+3+4}), 27.2 (dd, ^{2}J = 12.0, 4.0 Hz, CH_2 PCy_2 C_{2+3+4}), 27.7 (dd, ^{2}J = 15.0, 12.9 Hz, CH_2 PCy_2 C_{2+3+4}), 29.1 (s, CH_2 PCy_2 C_{2+3+4}), 29.5 (s, ^{t}Bu $C(CH_3)_3$), 29.5 (s, ^{t}Bu $C(CH_3)_3$), 29.8 (d, ^{2}J = 41.8 Hz, CH Ind), 31.0 (d, ^{2}J = 47.0 Hz, CH Ind), 34.6 (d, ^{2}J = 4.5 Hz, ^{t}Bu $C(CH_3)_3$), 41.2 (dd, $^{1}J_{CP}$ = 52.2 Hz, ^{2}J = 26.6 Hz, CH PCy_2 C_1), 64.8 (d, ^{2}J = 3.5 Hz, CH Ind), 107.9 (d, ^{2}J = 5.8 Hz, CH Ind), 117.8 (dd, $^{1}J_{CP}$ = 88.9 Hz,^{2}J = 5.3 Hz, C Pos. 6), 118.0(s, CH Ind), 120.5 (s, CH Ind), 121.7 (d, ^{2}J = 9.1 Hz, CH Pos. 4), 122.4 (d, ^{2}J = 6.6 Hz, CH Pos. 3), 124.71 (d, ^{2}J = 63.4 Hz, CH Ind), 125.9 (d, ^{2}J = 23.2 Hz, C Ind), 129.0 (d, ^{2}J = 2.2 Hz, CH Pos. 2), 130.4 (d, ^{2}J = 9.2 Hz, CH Pos. 1), 138.7 (d, ^{2}J = 5.4 Hz, C Ind), 140.3 (s, C Ind), 152.1 (dd, $^{3}J_{CP}$ = 14.8 Hz, ^{2}J = 3.5 Hz, C Pos. 5). ^{31}P NMR (162 MHz, C_6D_6) δ = 27.0 (d, $^{2}J_{PP}$ = 55.8 Hz, PCy_2), 56.7 (d, $^{2}J_{PP}$ = 56.0 Hz, *P*CS). IR (ATR) [cm^{-1}]: 2926 (m), 2843 (w), 1444 (m), 1362 (w), 1275 (w), 1196 (s), 1104 (m), 1060 (s), 1046 (m), 873 (m), 743 (s), 687 (m), 628 (w), 511 (m), 461 (s), 426 (s). CHNS for $C_{38}H_{55}ClP_2PdS$: Calcd: C: 61.04, H: 7.66, S: 4.74. Measured: C: 61.27, H: 7.89, S: 4.49. Melting point: 155.3 °C (decomposition).

*Synthesis of 9-Methyl-fluorene (**9-Me-Fluorene**)*. Following a slightly modified literature procedure,[27] 4.99 g (30 mmol) of fluorene was dissolved in 60 mL of THF and cooled to −60 °C. To this was slowly added (over a period of 15 min) 26 mL of a 1.55 M solution of *n*BuLi in hexane. The solution was warmed to room temperature and stirred for 1.5 h. The solution was cooled to −60 °C, and 2.8 mL (6.39 mg, 45 mmol) of MeI was added slowly over 5 min. The solution became clear and colorless and was then stirred for 15 min at −60 °C and 2 h at room temperature. Excess MeI was quenched with 100 mL of aqueous KOH solution. The aqueous phase was separated and extracted (2 × 5 mL) with Et_2O. The combined organic phases were dried with $MgSO_4$, and the solvent was removed. The crude product was filtered over a short silica column with hexane as eluent. The product was obtained as a yellow waxlike solid in 91% yield (5.0 g, 27.4 mmol). ^{1}H NMR (400 MHz, THF-d_8): δ [ppm] = 1.44 (d, 3H, ^{3}J = 7.34 Hz, CH_3), 3.85 (q, 1H, ^{3}J = 7.30 Hz, 9*H*Flu), 7.26 (m, 4H, Ar), 7.42 (d, 2H, ^{3}J = 7.15 Hz, Ar), 7.67 (m, 2H, Ar).[27]

Synthesis of ***ClPCyFlu***. First, 5.00 g (27.4 mmol) of **9-Me-Fluorene** was dissolved in 110 mL of THF and cooled to −60 °C. 17.7 mL of a 1.55 M solution of *n*BuLi in hexane was added slowly over 15 min. The solution turned red and was stirred for 30 min at 60 °C, before being cooled and stirred for 2 h at room temperature. A second solution of 4.2 mL (29 mmol, 5.07 g) of $PCyCl_2$ in 40 mL of THF was prepared and cooled to −60 °C. The lithiated **9-Me-**

https://doi.org/10.1021/acs.organomet.1c00349
Organometallics 2021, 40, 2888−2900

Fluorene solution was cooled to −60 °C and slowly added to the chlorophosphine solution over a period of 30 min. This was then stirred for 30 min at −60 °C and allowed to come to room temperature overnight. The solvent was removed, and the residue was suspended in 20 mL of hexane and filtered over Celite. The solvent was removed *in vacuo*, and the crude product purified by distillation (1×10^{-3} bar at 147 °C). Yield was not determined. ^{1}H NMR (400 MHz, DCM-d_2): δ [ppm] = 0.40 (m, 1H, PCy_2 CH_2 H_{2+3+4}), 0.5−1.0 (m, 6H, PCy_2 CH_2 + CH $H_{1+2+3+4}$), 1.2−1.4 (m, 3H, PCy_2 CH_2 H_{2+3+4}), 1.48 (s, 1H, PCy_2 CH_2 H_{2+3+4}), 1.86 (d, $^3J_{HP}$ = 13.3 Hz, CH_3). ^{13}C{^{1}H} NMR (100.6 MHz, DCM-d_2): δ [ppm] = 23.5 (d, $^3J_{CP}$ = 21.6 Hz, CH_3 Flu), 26.1 (d, ^2J = 1.43 Hz, CH_2 Cy C_{3+4}), 26.7 (d, $^2J_{CP}$ = 8.98 Hz, CH_2 Cy C_2), 26.8 (d, ^2J = 1.37 Hz, CH_2 Cy C_{3+4}), 28.8 (d, 6.26 Hz, CH_2 Cy H_{3+4}), 30.0 (d, $^2J_{CP}$ = 26.5 Hz, CH_2 Cy C_2), 38.5 (d, $^1J_{CP}$ = 38.5 Hz, CH Cy C_1), 53.0 (d, $^1J_{CP}$ = 41.1 Hz, C Flu_9). IR (ATR) [cm^{-1}]: 2917 (m), 2849 (s), 1474 (s), 1437 (m), 1026 (s), 763 (s), 742 (s), 729 (s), 603 (w), 565 (w), 473 (s), 453 (s), 423 (w). CHNS for $C_{20}H_{22}ClP$: Calcd: C: 73.06, H: 6.74. Measured: C: 73.05, H: 6.81. Melting point: 69.2 °C.

Synthesis of ***L2***. First, 1g (2.73 mmol) of phosphonium salt **1** and 306 mg (2.73 mmol) of KO*t*-Bu were suspended in 8 mL of THF and stirred for 4 h, forming a red solution. The solvent was removed *in vacuo*, and the residue was redissolved in 8 mL of pentane. The solution was subsequently filtered, and the solvent was removed. The residue was dissolved in 8 mL of THF and cooled to 0 °C. A solution of 449 mg of ClPCyFlu (0.5 equiv, 1.37 mmol) in 1 mL of THF was added slowly. A beige solid immediately precipitated from the solution. The solution was stirred for 2 h at room temperature and filtered, and the solvent was removed *in vacuo*. The residue was suspended in 15 mL of hot acetonitrile and stirred until dissolution. The solution was filtered while hot and allowed to slowly cool room temperature, precipitating a yellow solid. The solution was filtered, and the remaining solid was washed (3 × 1.5 mL) with acetonitrile. Phosphine **L2** was obtained as this yellow solid in 65% yield (940 g, 1.8 mmol). ^{1}H NMR (400 MHz, THF-d_8) δ = 0.27−0.55 (m, 3H, Cy CH_2 H_{2+3+4}), 0.67 (m, 3H, Cy CH_2 H_{2+3+4}), 0.84−1.08 (m, 9H, *i*Pr CH_3), 1.14 (m, 1H, Cy CH H_{2+3+4}), 1.23 (m, 2H, Cy CH_2 H_{2+3+4} + CH H_1), 1.32 (dd, ^3J = 16.1, 7.2 Hz, 3H, *i*Pr CH_3), 1.37 (s, 1H, Cy CH_2 H_{2+3+4}), 1.48 (d, ^3J = 11.8 Hz, 3H, Flu CH_3HH), 1.51 (s, 1H, Cy CH_2 H_{2+3+4}), 1.97 (dp, ^3J = 10.8, 7.1 Hz, 1H, *i*Pr CH), 2.61 (dp, ^3J = 10.6, 7.1 Hz, 1H, *i*Pr CH), 6.85 (m, 1H, CH Pos. 4), 6.98−7.08 (m, 5H, CH Pos. 2, CH Flu), 7.10 (m, 1H, CH Pos. 1*h*), 7.27 (m, 1H, CH Pos. 3), 7.33−7.39 (m, 1H, CH Flu), 7.43−7.50 (m, 1H, CH Flu), 7.51 (d, ^3J = 7.4 Hz, 1H, CH Flu), 7.75 (d, ^3J = 7.4 Hz, 1H, CH Flu). ^{13}C{^{1}H} NMR (100.6 MHz, DCM-d_2): δ [ppm] = 9.4 (dd, $^1J_{CP}$ = 42.8, 103.6 Hz, PCS), 16.7 (t, $^2J_{CP}$ = 2.51 Hz, *i*Pr CH_3), 17.6 (d, $^2J_{CP}$ = 2.6 Hz, *i*Pr CH_3), 17.8 (dd, $^2J_{CP}$ = 2.32, 12.7 Hz, *i*Pr CH_3), 18.1 (t, $^2J_{CP}$ = 2.56 Hz, *i*Pr CH_3), 25.9 (m, CH_2 Cy C_{2+3+4}), 27.6 (s, CH_3 Flu), 28.6 (d, ^2J = 7.78 Hz, CH_2 Cy C_{2+3+4}), 27.4 (d, $^2J_{CP}$ = 17.8 Hz, CH_2 Cy C_{2+3+4}), 32.3 (d, ^2J = 6.95 Hz, CH Cy C_{2+3+4}), 32.7 (d, $^2J_{CP}$ = 22.8 Hz, CH_2 Cy C_{2+3+4}), 27.9 (d, $^2J_{CP}$ = 47.9 Hz, CH *i*Pr), 33.9 (d, $^2J_{CP}$ = 46.4 Hz, CH *i*Pr), 37.3 (dd, $^2J_{CP}$ = 6.55, 10.4 Hz, CH_2 Cy C_1), 55.6 (dd, $^2J_{CP}$ = 3.27 Hz, ^2J = 30.4 Hz, CCH_3 Flu_9), 118.7 (dd, $^1J_{CP}$ = 90.5 Hz, ^2J = 7.24 Hz, C Pos. 6), 120.5 (d, ^2J = 18.8 Hz, CH Flu), 123.3 (d, $^2J_{CP}$ = 9.01 Hz, CH Pos. 4), 124.0 (d, ^2J = 6.97 Hz, CH Flu), 125.5 (d, $^2J_{CP}$ = 10.5 Hz, CH Pos. 1), 126.9 (dd, ^2J = 8.45, 1.77 Hz, CH Flu), 127.4 (d, ^2J = 4.11 Hz, CH Flu), 129.6 (d, ^2J = 9.32 Hz, CH Pos. 3), 130.2 (d, ^2J = 2.18 Hz, CH Pos. 2), 141.1 (d, $^2J_{CP}$ = 3.44 Hz, C Flu_{10+11}), 141.3 (s, C Flu_{12+13}), 155.8 (dd, $^2J_{CP}$ = 18.3 Hz, ^2J = 1.10 Hz, C Pos. 5). ^{31}P{^{1}H} NMR (162.1 MHz, THF-d_8): δ [ppm] = 12.2 (d, $^2J_{PP}$ = 119.5 Hz, PCyFlu), 52.0 (d, $^2J_{PP}$ = 119.5 Hz, *P*CS). IR (ATR) [cm^{-1}]: 2912 (w), 1439 (m), 1255 (w), 1103 (m), 1056 (m), 1023 (m), 868 (w), 808 (w), 757 (s), 739 (s), 729 (s), 666 (w), 636 (m), 571 (w), 447s, 426 (m). CHNS for $C_{33}H_{40}P_2S$: Calcd: C: 74.69, H: 7.60, S: 6.04. Measured: C: 74.23, H: 7.51, S: 5.69. Melting point: 76.2 °C (degradation).

Synthesis of ***Pd$_{al}$2***. First, 300 mg (0.565 mmol) of **L2** and 106 mg of $[Pd(allyl)Cl]_2$ (56.4 m% Pd, 0.283 mmol) were suspended in 8 mL of pentane and stirred for 2 h. After this time, the yellow suspension formed was filtered and the solid washed (2 × 5 mL) with pentane. Complex **Pd$_{al}$2** was obtained as a yellow solid in 73% yield (295 mg, 0.414 mmol). By slow diffusion of pentane into a solution of **Pd$_{al}$2** in THF-d_8, crystals suitable for single-crystal XRD could be obtained. (The obtained molecular structures and NMR data suggest two different conformers in solid state and solution.) ^{31}P{^{1}H} NMR (162.1 MHz, THF-d_8): δ [ppm] = 34.5 (d, $^2J_{PP}$ = 63.4 Hz, *P*CyFlu), 35.4 (d, $^2J_{PP}$ = 63.3 Hz, *P*CyFlu), 59.0 (d, $^2J_{PP}$ = 62.8 Hz, *P*CS), 59.1 (d, $^2J_{PP}$ = 63.4 Hz, *P*CS). ^{1}H NMR and ^{13}C NMR could not be evaluated due to the presence of two different conformers in solution. IR (ATR) [cm^{-1}]: 2916 (w), 1441 (m), 1105 (m), 1048 (m), 1013 (m), 866 (m), 739 (s), 727 (s), 687 (s), 631 (m), 571 (w), 448 (s), 425 (m). Melting point: 133.7 °C (degradation). CHNS for $C_{36}H_{45}ClP_2PdS$: Calcd: C: 60.59, H: 6.36, S: 4.49. Measured: C: 59.74, H: 6.20, S: 4.19

Synthesis of ***Pd$_{cin}$2***. First, 300 mg (0.565 mmol) of **L2** and 149 mg of $[Pd(cinnamyl)Cl]_2$ (40.2 m% Pd, 0.283 mmol) were suspended in 8 mL of pentane and stirred for 2 h. The orange suspension formed was filtered, and the solid was washed (2 × 5 mL) with pentane. Complex **Pd$_{cin}$2**was obtained as an orange solid in 76% yield (340 mg, 0.431 mmol). By slow diffusion of pentane into a solution of **Pd$_{cin}$2** in THF-d_8, crystals suitable for X-ray diffraction could be obtained. (The obtained molecular structures and NMR data suggest two different conformers in solid state and solution.) ^{31}P{^{1}H} NMR (162.1 MHz, THF-d_8): δ [ppm] = 37.3 (d, $^2J_{PP}$ = 62.7 Hz, *P*CyFlu), 39.2 (d, $^2J_{PP}$ = 62.57 Hz, *P*CyFlu), 59.10 (d, $^2J_{PP}$ = 63.13 Hz, *P*CS), 59.24 (d, $^2J_{PP}$ = 62.49 Hz, *P*CS). ^{1}H NMR and ^{13}C NMR could not be evaluated due to the presence of two different conformers in solution. IR (ATR) [cm^{-1}]: 2922 (w), 1443 (m), 1110 (w), 1037 (m), 869 (m), 763 (w), 728 (s), 689 (s), 653 (m), 623 (w), 511 (w), 452 (m). Melting point: 159.2 °C (degradation).

Synthesis of ***Pd$_{ind}$2***. First, 120 mg (0.23 mmol) of **L2** and 72.4 mg of $[Pd(^tBu\text{-}Indenyl)Cl]_2$ (33.2 m% Pd, 0.12 mmol) were suspended in 4 mL of pentane and stirred for 2 h. A dark brown suspension formed, which was subsequently filtered, and the solid was washed (2 × 5 mL) with pentane. Complex **Pd$_{ind}$2** was obtained as brown solid in 66% yield (127 mg). By slow diffusion of pentane into a solution in THF-d_8, crystals suitable for single-crystal XRD could be obtained. (The obtained molecular structures and NMR data suggest two different conformers in solid state and solution.) ^{31}P{^{1}H} NMR (162.1 MHz, THF-d_8): δ [ppm] = 40.80 (d, $^2J_{PP}$ = 56.7 Hz, *P*CyFlu), 44.5 (d, $^2J_{PP}$ = 56.6 Hz, *P*CyFlu), 58.4 (d, $^2J_{PP}$ = 56.8 Hz, *P*CS), 60.3 (d, $^2J_{PP}$ = 56.7 Hz, *P*CS). ^{1}H NMR and ^{13}C NMR could not be evaluated due to the presence of two different conformers in solution. IR (ATR) [cm^{-1}]: 2916 (m), 1444 (m), 1363 (w), 1106 (m), 1025 (s), 861 (m), 737 (s), 654 (m), 621 (w), 601 (w), 463 (m), 448 (m). Melting point: 148.8 °C (degradation).

Computational Details. All calculations were performed without symmetry restrictions. Starting coordinates obtained with GaussView 6.0[28] or directly from the crystal structure analyses for synthesized ligands. The geometry optimization and NBO[29] analysis were carried out with the Gaussian16 (revision C.01)[30] program package, and the AIM analysis was done with the Multiwfn program version 3.6.[31] The geometry optimization and AIM analysis of the palladium complex was performed using density functional theory (DFT)[32,33] with the PBE0 functional,[34] through the LANL2TZ(f) basis set and the corresponding ECP for palladium[35−37] and the def2svp basis set[38] for all other atoms, in conjunction with Grimme's D3 dispersion correction with Becke−Johnson damping.[39−41] For the examined ligands, geometry optimizations were performed using DFT with B3LYP-D3/6-31+G*.[42−47] The metrical parameters of the energy-optimized geometries are in good agreement with those determined by X-ray diffraction. Harmonic vibrational frequency analyses were performed at the same level of theory as the optimizations to determine the nature of the structure.[48] The vibrational frequency analysis showed no imaginary frequencies. The NBO analysis was performed with the B3LYP functional, the LANL2TZ(f) basis set, and the corresponding ECP for palladium and the 6-31+G* basis set for all other atoms. The charges were fit to the electrostatic potential at points selected according to the CHelp scheme and the electrostatic

https://doi.org/10.1021/acs.organomet.1c00349
Organometallics 2021, 40, 2888−2900

property for the phosphorus atom of the phosphine was taken from that fit.[49]

Crystallographic Details. Data collection of all compounds was carried out on either an Oxford SuperNova diffractometer (Cu microsource) or an XtaLAB Synergy (HyPix detector). Suitable crystals of all compounds were mounted in an inert oil (perfluoropoly aklylether) and directly transferred into a cold nitrogen stream. All crystal structure determinations were carried out at 100 K. The structures were solved using direct methods, refined using full-matrix least-squares techniques on F^2 with the SHELX software package[50,51] and expanded using Fourier techniques. Data collection parameters are given in Tables S1–S4. Crystallographic data (including structural factors) have been deposited with the Cambridge Crystallographic Data Centre as supplementary publication CCDC numbers 2089207–2089217.

■ ASSOCIATED CONTENT

Supporting Information

The Supporting Information is available free of charge at https://pubs.acs.org/doi/10.1021/acs.organomet.1c00349.

NMR spectra, crystallographic and computational details (PDF)

Coordinates of the energy-optimized structures (XYZ)

Accession Codes

CCDC 2089207–2089217 contain the supplementary crystallographic data for this paper. These data can be obtained free of charge via www.ccdc.cam.ac.uk/data_request/cif, or by emailing data_request@ccdc.cam.ac.uk, or by contacting The Cambridge Crystallographic Data Centre, 12 Union Road, Cambridge CB2 1EZ, UK; fax: +44 1223 336033.

■ AUTHOR INFORMATION

Corresponding Author

Viktoria H. Gessner − *Chair of Inorganic Chemistry II, Faculty of Chemistry and Biochemistry, Ruhr-Universität Bochum, 44801 Bochum, Germany;* orcid.org/0000-0001-6557-2366; Email: viktoria.gessner@rub.de

Authors

Julian Löffler − *Chair of Inorganic Chemistry II, Faculty of Chemistry and Biochemistry, Ruhr-Universität Bochum, 44801 Bochum, Germany*

Richard M. Gauld − *Chair of Inorganic Chemistry II, Faculty of Chemistry and Biochemistry, Ruhr-Universität Bochum, 44801 Bochum, Germany*

Kai-Stephan Feichtner − *Chair of Inorganic Chemistry II, Faculty of Chemistry and Biochemistry, Ruhr-Universität Bochum, 44801 Bochum, Germany*

Ilja Rodstein − *Chair of Inorganic Chemistry II, Faculty of Chemistry and Biochemistry, Ruhr-Universität Bochum, 44801 Bochum, Germany*

Jana-Alina Zur − *Chair of Inorganic Chemistry II, Faculty of Chemistry and Biochemistry, Ruhr-Universität Bochum, 44801 Bochum, Germany*

Jens Handelmann − *Chair of Inorganic Chemistry II, Faculty of Chemistry and Biochemistry, Ruhr-Universität Bochum, 44801 Bochum, Germany*

Christopher Schwarz − *Chair of Inorganic Chemistry II, Faculty of Chemistry and Biochemistry, Ruhr-Universität Bochum, 44801 Bochum, Germany*

Complete contact information is available at: https://pubs.acs.org/10.1021/acs.organomet.1c00349

Notes

The authors declare the following competing financial interest(s): The authors have filed patent WO2019030304 covering the YPhos ligands and precatalysts discussed, which is held by UMICORE, and products will be made commercially available.

■ ACKNOWLEDGMENTS

This work was supported by RESOLV, funded by the Deutsche Forschungsgemeinschaft (DFG, German Research Foundation) under Germany's Excellence Strategy - EXC-2033 - Projektnummer 390677874 and by the European Research Council (Starting Grant: YlideLigands 677749). We also thank UMICORE AG & Co. KG for financial support and the donation of chemicals.

■ REFERENCES

(1) (a) Ruiz-Castillo, P.; Buchwald, S. L. Applications of Palladium-Catalyzed C–N Cross-Coupling Reactions. *Chem. Rev.* **2016**, *116*, 12564–12649. (b) Dorel, R.; Grugel, C. P.; Haydl, A. The Buchwald–Hartwig Amination After 25 Years. *Angew. Chem., Int. Ed.* **2019**, *58*, 17118–17129. (c) Buchwald, S. L.; Mauger, C.; Mignani, G.; Scholz, U. Industrial-Scale Palladium-Catalyzed Coupling of Aryl Halides and Amines − A Personal Account. *Adv. Synth. Catal.* **2006**, *348*, 23–39.

(2) (a) Torborg, C.; Beller, M. Recent Applications of Palladium-Catalyzed Coupling Reactions in the Pharmaceutical, Agrochemical, and Fine Chemical Industries. *Adv. Synth. Catal.* **2009**, *351*, 3027–3043. (b) Hartwig, J. F. Evolution of a Fourth Generation Catalyst for the Amination and Thioetherification of Aryl Halides. *Acc. Chem. Res.* **2008**, *41*, 1534–1544. (c) Marion, N.; Nolan, S. P. Well-Defined N-Heterocyclic Carbenes–Palladium(II) Precatalysts for Cross-Coupling Reactions. *Acc. Chem. Res.* **2008**, *41*, 1440–1449. (d) Fu, G. C. The Development of Versatile Methods for Palladium-Catalyzed Coupling Reactions of Aryl Electrophiles through the Use of P(*t*-Bu)$_3$ and PCy$_3$ as Ligands. *Acc. Chem. Res.* **2008**, *41*, 1555–1564. (e) Würtz, S.; Glorius, F. Surveying Sterically Demanding N-Heterocyclic Carbene Ligands with Restricted Flexibility for Palladium-catalyzed Cross-Coupling Reactions. *Acc. Chem. Res.* **2008**, *41*, 1523–1533. (f) Martin, R.; Buchwald, S. L. Palladium-Catalyzed Suzuki–Miyaura Cross-Coupling Reactions Employing Dialkylbiaryl Phosphine Ligands. *Acc. Chem. Res.* **2008**, *41*, 1461–1473. (g) Johansson Seechurn, C. C. C.; Kitching, M. O.; Colacot, T. J.; Snieckus, V. Palladium-Catalyzed Cross-Coupling: A Historical Contextual Perspective to the 2010 Nobel Prize. *Angew. Chem., Int. Ed.* **2012**, *51*, 5062–5085. (h) Li, H.; Johansson Seechurn, C. C. C.; Colacot, T. J. Development of Preformed Pd Catalysts for Cross-Coupling Reactions, Beyond the 2010 Nobel Prize. *ACS Catal.* **2012**, *2*, 1147–1164. (i) Valente, C.; Calimsiz, S.; Hoi, K. H.; Mallik, D.; Sayah, M.; Organ, M. G. The Development of Bulky Palladium NHC Complexes for the Most-Challenging Cross-Coupling Reactions. *Angew. Chem., Int. Ed.* **2012**, *51*, 3314–3332.

(3) Guo, H.; Fan, Y. C.; Sun, Z.; Wu, Y.; Kwon, O. Phosphine Organocatalysis. *Chem. Rev.* **2018**, *118*, 10049–10293.

(4) Allen, D. W. Phosphines and related P–C-bonded compounds. *Organophosphorus Chem.* **2014**, *43*, 1–51.

(5) Saunders, A. J.; Crossley, I. R.; Roe, S. M. Arylphosphanes: Base-Free Synthesis and Their Coordination Chemistry with Platinum-Group Metals. *Eur. J. Inorg. Chem.* **2016**, *2016*, 4076.

(6) (a) Strohmeier, W.; Müller, F.-J. Klassifizierung phosphorhaltiger Liganden in Metallcarbonyl-Derivaten nach der π-Acceptorstärke. *Chem. Ber.* **1967**, *100*, 2812–2821. (b) Tolman, C. A. Electron donor-acceptor properties of phosphorus ligands. Substituent additivity. *J. Am. Chem. Soc.* **1970**, *92*, 2953–2956.

(7) Tolman, C. A. Phosphorus ligand exchange equilibriums on zerovalent nickel. Dominant role for steric effects. *J. Am. Chem. Soc.* **1970**, *92*, 2956–2965.

(8) Clavier, H.; Nolan, S. P. Percent buried volume for phosphine and N-heterocyclic carbene ligands: steric properties in organometallic chemistry. *Chem. Commun.* **2010**, *46*, 841−861.
(9) (a) Reid, J. P.; Sigman, M. S. Holistic Prediction of Enantioselectivity in Asymmetric Catalysis. *Nature* **2019**, *571*, 343−348. (b) Durand, D. J.; Fey, N. Computational Ligand Descriptors for Catalyst Design. *Chem. Rev.* **2019**, *119*, 6561−6594. (c) Gensch, T.; dos Passos Gomes, G.; Friederich, P.; Peters, E.; Gaudin, T.; Pollice, R.; Jorner, K.; Nigman, A.; Lindner-D'Addario, M.; Sigman, M. S.; Aspuru-Guzik, A. A comprehensive discovery platform for organophosphorus ligands for catalysis. *ChemRxiv (Theoretical and Computational Chemistry)*, April 27, 2021, DOI: 10.26434/chemrxiv.12996665.v1.
(10) (a) Chen, L.; Ren, P.; Carrow, B. P. Tri(1-adamantyl)phosphine: Expanding the Boundary of Electron-Releasing Character Available to Organophosphorus Compounds. *J. Am. Chem. Soc.* **2016**, *138*, 6392−6395. (b) Chen, L.; Sanchez, D. R.; Zhang, B.; Carrow, B. P. Cationic" Suzuki−Miyaura Coupling with Acutely Base-Sensitive Boronic Acids. *J. Am. Chem. Soc.* **2017**, *139*, 12418−12421.
(11) (a) Wünsche, M. A.; Mehlmann, P.; Witteler, T.; Buß, F.; Rathmann, P.; Dielmann, F. Imidazolin-2-ylidenaminophosphines as Highly Electron-Rich Ligands for Transition-Metal Catalysts. *Angew. Chem., Int. Ed.* **2015**, *54*, 11857. (b) Buß, F.; Mehlmann, P.; Mück-Lichtenfeld, C.; Bergander, K.; Dielmann, F. Reversible Carbon Dioxide Binding by Simple Lewis Base Adducts with Electron-Rich Phosphines. *J. Am. Chem. Soc.* **2016**, *138*, 1840−1843. (c) Mehlmann, P.; Mück-Lichtenfeld, C.; Tan, T. T. Y.; Dielmann, F. Tris(imidazolin-2-ylidenamino)phosphine: A Crystalline Phosphorus(III) Superbase That Splits Carbon Dioxide. *Chem. - Eur. J.* **2017**, *23*, 5929−5933.
(12) Ullrich, S.; Kovačević, B.; Xie, X.; Sundermeyer, J. Phosphazenyl Phosphines: The Most Electron-Rich Uncharged Phosphorus Brønsted and Lewis Bases. *Angew. Chem., Int. Ed.* **2019**, *58*, 10335−10339.
(13) (a) Scherpf, T.; Schwarz, C.; Scharf, L. T.; Zur, J.-A.; Helbig, A.; Gessner, V. H. Ylide-Functionalized Phosphines: Strong Donor Ligands for Homogeneous Catalysis. *Angew. Chem., Int. Ed.* **2018**, *57*, 12859−12864. (b) Scherpf, T.; Rodstein, I.; Paassen, M.; Gessner, V. H. Group 9 and 10 Metal Complexes of an Ylide-Substituted Phosphine: Coordination versus Cyclometalation and Oxidative Addition. *Inorg. Chem.* **2019**, *58*, 8151−8161.
(14) (a) Schwarz, C.; Handelmann, J.; Baier, D. M.; Ouissa, A.; Gessner, V. H. Mono- and diylide-substituted phosphines (YPhos): impact of the ligand properties on the catalytic activity in gold(I)-catalysed hydroaminations. *Catal. Sci. Technol.* **2019**, *9*, 6808−6815. (b) Handelmann, J.; Babu, C. N.; Steinert, H.; Schwarz, C.; Scherpf, T.; Kroll, A.; Gessner, V. H. Towards the Rational Design of Ylide-Substituted Phosphines for Gold(I)-Catalysis: From Inactive to ppm-level Catalysis. *Chem. Sci.* **2021**, *12*, 4329−4337.
(15) (a) Weber, P.; Scherpf, T.; Rodstein, I.; Lichte, D.; Scharf, L. T.; Gooßen, L. J.; Gessner, V. H. A Highly Active Ylide-Functionalized Phosphine for Palladium-Catalyzed Aminations of Aryl Chlorides. *Angew. Chem., Int. Ed.* **2019**, *58*, 3203−3207. (b) Scherpf, T.; Steinert, H.; Großjohann, A.; Dilchert, K.; Tappen, J.; Rodstein, I.; Gessner, V. H. Efficient Pd-Catalyzed Direct Coupling of Aryl Chlorides with Alkyllithium Reagents. *Angew. Chem., Int. Ed.* **2020**, *59*, 20596−20603. (c) Hu, Z.; Wei, X.-J.; Handelmann, J.; Seitz, A.-K.; Rodstein, I.; Gessner, V. H.; Gooßen, L. J. Coupling of Reformatsky Reagents with Aryl Chlorides enabled by Ylide-Functionalized Phosphine Ligands. *Angew. Chem., Int. Ed.* **2021**, *60*, 6778−6783. (d) Rodstein, I.; Prendes, D. S.; Wickert, L.; Paaßen, M.; Gessner, V. H. Selective Monoarylation of Small Primary Alkyl Amines through Backbone-Modification in Ylide-Functionalized Phosphines (YPhos). *J. Org. Chem.* **2020**, *85*, 14674−14683.
(16) Scharf, L. T.; Rodstein, I.; Schmidt, M.; Scherpf, T.; Gessner, V. H. Unraveling the High Activity of Ylide-Functionalized Phosphines in Palladium-Catalyzed Amination Reactions: A Comparative Study with ^{Cy}JohnPhos and PtBu$_3$. *ACS Catal.* **2020**, *10*, 999−1009.
(17) (a) Weber, P.; Biafora, A.; Doppiu, A.; Bongard, H.-J.; Kelm, H.; Gooßen, L. J. A comparative study of dibenzylideneacetone palladium complexes in catalysis. *Org. Process Res. Dev.* **2019**, *23*, 1462−1470. (b) Zalesskiy, S. S.; Ananikov, V. P. $Pd_2(dba)_3$ as a Precursor of Soluble Metal Complexes and Nanoparticles: Determination of Palladium Active Species for Catalysis and Synthesis. *Organometallics* **2012**, *31*, 2302−2309.
(18) (a) Poater, A.; Cosenza, B.; Correa, A.; Giudice, S.; Ragone, F.; Scarano, V.; Cavallo, L. SambVca: A Web Application for the Calculation of the Buried Volume of N-Heterocyclic Carbene Ligands. *Eur. J. Inorg. Chem.* **2009**, *2009*, 1759−1766. (b) Falivene, L.; Cao, Z.; Petta, A.; Serra, L.; Poater, A.; Oliva, R.; Scarano, V.; Cavallo, L. Towards the online computer-aided design of catalytic pockets. *Nat. Chem.* **2019**, *11*, 872−879.
(19) Christmann, U.; Vilar, R. Monoligated Palladium Species as Catalysts in Cross-Coupling Reactions. *Angew. Chem., Int. Ed.* **2005**, *44*, 366−374.
(20) Hazari, N.; Melvin, P. R.; Beromi, M. M. Well-defined nickel and palladium precatalysts for cross-coupling. *Nat. Rev. Chem.* **2017**, *1*, 25.
(21) (a) Chartoire, A.; Frogneux, X.; Nolan, S. P. An Efficient Palladium-NHC (NHC = N-Heterocyclic Carbene) and Aryl Amination Pre-Catalyst: [Pd(IPr*)(cinnamyl)Cl]. *Adv. Synth. Catal.* **2012**, *354*, 1897−1901. (b) Melvin, P. R.; Nova, A.; Balcells, D.; Dai, W.; Hazari, N.; Hruszkewycz, D. P.; Shah, H. P.; Tudge, M. T. Design of a Versatile and Improved Precatalyst Scaffold for Palladium-Catalyzed Cross-Coupling: (η^3-1-^{t}Bu-indenyl)$_2$(μ-Cl)$_2$Pd$_2$ Rapidly Activating Pd-Precatalyst for Suzuki−Miyaura and Buchwald−Hartwig Couplings of Aryl Esters. *ACS Catal.* **2015**, *5*, 3680−3688. (c) Johansson Seechurn, C. C. C.; Parisel, S. L.; Colacot, T. J. Air-Stable Pd(R-allyl)LCl (L= Q-Phos, P(t-Bu)$_3$, etc.) Systems for C−C/N Couplings: Insight into the Structure−Activity Relationship and Catalyst Activation Pathway. *J. Org. Chem.* **2011**, *76*, 7918−7932. (d) Tappen, J.; Rodstein, I.; McGuire, K.; Großjohann, A.; Löffler, J.; Scherpf, T.; Gessner, V. H. Palladium Complexes Based on Ylide-Functionalized Phosphines (YPhos): Broadly Applicable High-Performance Precatalysts for the Amination of Aryl Halides at Room Temperature. *Chem. - Eur. J.* **2020**, *26*, 4281−4288. (e) Biscoe, M. R.; Fors, B. P.; Buchwald, S. L. A New Class of Easily Activated Palladium Precatalysts for Facile C−N Cross-Coupling Reactions and the Low Temperature Oxidative Addition of Aryl Chlorides. *J. Am. Chem. Soc.* **2008**, *130*, 6686−6687. (f) O'Brien, C. J.; Kantchev, E. A. B.; Valente, C.; Hadei, N.; Chass, G. A.; Lough, A.; Hopkinson, A. C.; Organ, M. G. Easily Prepared Air- and Moisture-Stable Pd−NHC (NHC = N-Heterocyclic Carbene) Complexes: A Reliable, User-Friendly, Highly Active Palladium Precatalyst for the Suzuki−Miyaura Reaction. *Chem. - Eur. J.* **2006**, *12*, 4743−4748. (g) Viciu, M. S.; Germaneau, R. F.; Nolan, S. P. An Air-Stable Palladium/N-Heterocyclic Carbene Complex and Its Reactivity in Aryl Amination. *Org. Lett.* **2002**, *4*, 4053−4056. (h) Marion, N.; Navarro, O.; Mei, J.; Stevens, E. D.; Scott, N. M.; Nolan, S. P. Activation and Reactivity of (NHC)Pd(allyl)Cl (NHC = N-Heterocyclic Carbene) Complexes in Cross-Coupling Reactions. *J. Am. Chem. Soc.* **2006**, *128*, 4101−4111.
(22) Suresh, C. H.; Koga, N. Quantifying the Electronic Effect of Substituted Phosphine Ligands via Molecular Electrostatic Potential. *Inorg. Chem.* **2002**, *41*, 1573.
(23) Fleckenstein, C. A.; Plenio, H. 9-Fluorenylphosphines for the Pd-Catalyzed Sonogashira, Suzuki, and Buchwald−Hartwig Coupling Reactions in Organic Solvents and Water. *Chem. - Eur. J.* **2007**, *13*, 2701−2716.
(24) (a) Dunne, B. J.; Morris, R. B.; Orpen, A. G. Structural Systematics. Part 3. Geometry Deformations in Triphenylphosphine Fragments: a Test of Bonding Theories in Phosphine Complexes. *J. Chem. Soc., Dalton Trans.* **1991**, 653−661. (b) Orpen, A. G.; Connelly, N. G. Structural Systematics: Role of P-A σ^* Orbitals in Metal-Phosphorus π-Bonding in Redox-Related Pairs of M-PA$_3$ Complexes (A = R, Ar, OR; R = Alkyl). *Organometallics* **1990**, *9*, 1206−1210.
(25) (a) Faller, J. W.; Sarantopoulos, N. Retention of Configuration and Regiochemistry in Allylic Alkylations via the Memory Effect. *Organometallics* **2004**, *23*, 2179−2185. (b) Faller, J. W.;

https://doi.org/10.1021/acs.organomet.1c00349
Organometallics 2021, 40, 2888−2900

Sarantopoulos, N. Novel Binding Modes and Hemilability in Atropisomeric Phosphino−Amino Palladium Complexes. *Organometallics* **2004**, *23*, 2008−2014. (c) Walker, S. D.; Barder, T. E.; Martinelli, J. R.; Buchwald, S. L. A Rationally Designed Universal Catalyst for Suzuki−Miyaura Coupling Processes. *Angew. Chem., Int. Ed.* **2004**, *43*, 1871−1876.
(26) (a) Romanenko, V. D.; Tovstenko, V. I.; Markovski, L. N. Applications of Iodotrimethylsilane for the Synthesis of Iodophosphines, Iodophosphoranes, and Iodomethylphosphine Oxides. *Synthesis* **1980**, 823−825. (b) Uson, R.; Laguna, A.; Laguna, M.; Briggs, D. A.; Murray, H. H.; Fackler, J. P., Jr (Tetrahydrothiophene)Gold(I) or Gold(III) Complexes. *Inorg. Synth.* **2007**, *26*, 85−91.
(27) Fleckenstein, C. A.; Plenio, H. 9-Fluorenylphosphines for the Pd-Catalyzed Sonogashira, Suzuki, and Buchwald−Hartwig Coupling Reactions in Organic Solvents and Water. *Chem. - Eur. J.* **2007**, *13*, 2701−2716.
(28) Dennington, R.; Keith, T. A.; Millam, J. M. *GaussView*, version 6.1; Semichem Inc.: Shawnee Mission, KS, 2016.
(29) Glendening, E. D.; Badenhoop, J. K.; Reed, A. E.; Carpenter, J. E.; Bohmann, J. A.; Morales, C. M.; Karafiloglou, P.; Landis, C. R.; Weinhold, F. *NBO* 7.0; Theoretical Chemistry Institute, University of Wisconsin: Madison, WI, 2018.
(30) Frisch, M. J.; Trucks, G. W.; Schlegel, H. B.; Scuseria, G. E.; Robb, M. A.; Cheeseman, J. R.; Scalmani, G.; Barone, V.; Petersson, G. A.; Nakatsuji, H.; Li, X.; Caricato, M.; Marenich, A. V.; Bloino, J.; Janesko, B. G.; Gomperts, R.; Mennucci, B.; Hratchian, H. P.; Ortiz, J. V.; Izmaylov, A. F.; Sonnenberg, J. L.; Williams-Young, D.; Ding, F.; Lipparini, F.; Egidi, F.; Goings, J.; Peng, B.; Petrone, A.; Henderson, T.; Ranasinghe, D.; Zakrzewski, V. G.; Gao, J.; Rega, N.; Zheng, G.; Liang, W.; Hada, M.; Ehara, M.; Toyota, K.; Fukuda, R.; Hasegawa, J.; Ishida, M.; Nakajima, T.; Honda, Y.; Kitao, O.; Nakai, H.; Vreven, T.; Throssell, K.; Montgomery, J. A., Jr.; Peralta, J. E.; Ogliaro, F.; Bearpark, M.; Heyd, J. J.; Brothers, E. N.; Kudin, K. N.; Staroverov, V. N.; Kobayashi, R.; Normand, J.; Raghavachari, K.; Rendell, A.; Burant, J. C.; Iyengar, S. S.; Tomasi, J.; Cossi, M.; Millam, J. M.; Klene, M.; Adamo, C.; Cammi, R.; Ochterski, J. W.; Martin, R. L.; Morokuma, K.; Farkas, O.; Foresman, J. B.; Fox, D. J. *Gaussian 16*, revision C.01; Gaussian, Inc.: Wallingford CT, 2016.
(31) Lu, T.; Chen, F. Multiwfn: A Multifunctional Wavefunction Analyzer. *J. Comput. Chem.* **2012**, *33*, 580−592.
(32) Hohenberg, P.; Kohn, W. Inhomogeneous Electron Gas. *Phys. Rev.* **1964**, *136*, B864−B871.
(33) Kohn, W.; Sham, L. J. Self-Consistent Equations Including Exchange and Correlation Effects. *Phys. Rev.* **1965**, *140*, A1133−A1138.
(34) Adamo, C.; Barone, V. Toward reliable density functional methods without adjustable parameters: The PBE0 model. *J. Chem. Phys.* **1999**, *110*, 6158−6170.
(35) Hay, P. J.; Wadt, W. R. *Ab initio* effective core potentials for molecular calculations. Potentials for K to Au including the outermost core orbitals. *J. Chem. Phys.* **1985**, *82*, 299−310.
(36) Wadt, W. R.; Hay, P. J. *Ab initio* effective core potentials for molecular calculations. Potentials for main group elements Na to Bi. *J. Chem. Phys.* **1985**, *82*, 284−298.
(37) Hay, P. J.; Wadt, W. R. *Ab initio* effective core potentials for molecular calculations. Potentials for the transition metal atoms Sc to Hg. *J. Chem. Phys.* **1985**, *82*, 270−283.
(38) Weigend, F.; Ahlrichs, R. Balanced basis sets of split valence, triple zeta valence and quadruple zeta valence quality for H to Rn: Design and assessment of accuracy. *Phys. Chem. Chem. Phys.* **2005**, *7*, 3297−3305.
(39) Grimme, S.; Ehrlich, S.; Goerigk, L. Effect of the Damping Function in Dispersion Corrected Density Functional Theory. *J. Comput. Chem.* **2011**, *32*, 1456−1465.
(40) Grimme, S.; Antony, J.; Ehrlich, S.; Krieg, H. A consistent and accurate ab initio parametrization of density functional dispersion correction (DFT-D) for the 94 elements H-Pu. *J. Chem. Phys.* **2010**, *132*, 154104.
(41) Dolgonos, G. A.; Boese, A. D. Adjusting dispersion parameters for the density-functional tight-binding description of molecular crystals. *Chem. Phys. Lett.* **2019**, *718*, 7−11.
(42) Becke, A. D. Density-functional thermochemistry. III. The role of exact exchange. *J. Chem. Phys.* **1993**, *98*, 5648−5652.
(43) Lee, C.; Yang, W.; Parr, R. G. Development of the Colle-Salvetti correlation-energy formula into a functional of the electron density. *Phys. Rev. B: Condens. Matter Mater. Phys.* **1988**, *37*, 785−789.
(44) Vosko, S. H.; Wilk, L.; Nusair, M. Accurate spin-dependent electron liquid correlation energies for local spin density calculations: a critical analysis. *Can. J. Phys.* **1980**, *58*, 1200−1211.
(45) Stephens, P. J.; Devlin, F. J.; Chabalowski, C. F.; Frisch, M. J. Ab Initio Calculation of Vibrational Absorption and Circular Dichroism Spectra Using Density Functional Force Fields. *J. Phys. Chem.* **1994**, *98*, 11623−11627.
(46) McLean, A. D.; Chandler, G. S. Contracted Gaussian basis sets for molecular calculations. I. Second row atoms, Z = 11−18. *J. Chem. Phys.* **1980**, *72*, 5639−5648.
(47) Pople, J. A.; Head-Gordon, M.; Fox, D. J.; Raghavachari, K.; Curtiss, L. A. Gaussian-1 theory: A general procedure for prediction of molecular energies. *J. Chem. Phys.* **1989**, *90*, 5622−5629.
(48) Deglmann, P.; Furche, F.; Ahlrichs, R. An efficient implementation of second analytical derivatives for density functional methods. *Chem. Phys. Lett.* **2002**, *362*, 511−518.
(49) Chirlian, L. E.; Francl, M. M. Atomic charges derived from electrostatic potentials: A detailed study. *J. Comput. Chem.* **1987**, *8*, 894−905.
(50) Sheldrick, G. A short history of SHELX. *Acta Crystallogr., Sect. A: Found. Crystallogr.* **2008**, *64*, 112−122.
(51) Sheldrick, G. Crystal structure refinement with SHELXL. *Acta Crystallogr., Sect. C: Struct. Chem.* **2015**, *71*, 3−8.

https://doi.org/10.1021/acs.organomet.1c00349
Organometallics 2021, 40, 2888−2900